Addis Ababa University

School of Graduate Studies

SEISMOTECTONICS OF THE ETHIOPIAN RIFT FROM SOME SELECTED EARTHQUAKES IN 2001

Manahloh Belachew Yihun

July 2007

Addis Ababa

Seismotectonics of the Ethiopian Rift from some Selected Earthquakes in 2001

By

Manahloh Belachew Yihun

A Thesis Submitted To The School of Graduate Studies of The Addis Ababa University In Partial Fulfillment of The Requirements For The Degree of Masters of Science in Solid-Earth Geophysics

Department of Earth Sciences

Addis Ababa University

July 2007

Addis Ababa

Addis Ababa University

School of Graduate Studies

Seismotectonics of the Ethiopian Rift from some Selected Earthquakes in 2001

By

Manahloh Belachew Yihun

(Department of Earth Sciences)

Approved by Board of Examiners

_____ _____

Advisor

_____ _____

Examiner

_____ _____

Examiner

Acknowledgements

First of all I would like to thank God who gave me his blessings, health, great peace of heart and mind. I am deepely indebted to my advisor Dr. Atalay Ayele for his sound advice and encouragement. I appreciate the effort you made to make me acquainted with research culture.

I am also grateful to all staff members of the Geophysical Observatory for providing the friendly and a very pleasant atmosphere right from the start of my career at the Observatory.

My words are limited to express my feelings I have of Simegn. No one deserves more credit than you in relation to this work. I will always be grateful Sister. I would also like to take this opportunity to thank Bele for your care and support – you taught me what it means by good guidance of an elder brother. To my parents: you have been there and gave all your life to make us better persons – may God give you health and long life.

I thank my friends for their interest during all these years and for all the fun that we have had (and are going to have of course). Specially, Shimelis, Leta and Solomon - the support you offered me at various stages of this work is also appreciated.

Finally, I would like to thank IPPS (International Program for Physical Sciences) for the partial financial support for this study and also Addis Ababa University for the very small financial support.

Abstract

Earthquake data mainly between May and July 2001 are used in this study of the seismicity of the Main Ethiopian Rift system. The major source of data is the IRIS/PASSCAL (Incorporated Research Institutes of Seismology/Program for the Array Seismic Studies of the Continental Lithosphere) Broadband Seismic Experiment recently conducted in Ethiopia (Nyblade and Langston, 2002). This experiment was operational between 2000 and 2002. Hypocentral parameters for 144 earthquakes are determined using the location program Hypoinverse-2000. The locations stability is tested by relocating the earthquakes using the double-difference algorithm. The distribution of epicenters in this study shows high seismic activity around 9^0N and 40^0E, and 9.5^0N and 39.5^0E during the study period. These epicenters are close to the N-S trending Ankober border fault and Dofen volcano. Local magnitudes are estimated for the reported events. Fault plane solutions are determined for five selected earthquakes using the FOCMEC program and show pure normal faulting mechanisms. Four of these mechanisms, which were located near the Ankober Border Fault, show N-S trending fault orientation while the fifth solution for an earthquake from the western plateau has nodal planes trending NW-SE. On the other hand, three separate b-values are estimated using both the least-squares method and the maximum-likelihood method for the whole rift system and the high seismicity (Ankober-Dofen) area. For the whole rift under study, b-values of 1.059±0.13 were obtained using the maximum-likelihood method and 1.22 using the least-squares method. On the other hand, b-values of 1.17±0.16 and 1.37 using the maximum-likelihood and least-squares methods, respectively, are also determined for the highly seismic Ankober-Dofen region during the study period. By including magnitude data from another source for the year 2001 a separate b-value is also estimated for the region which experienced higher seismic activity - a maximum-likelihood

estimate of 0.81±0.05 and a least-squares estimate of 0.91 is obtained. The b-values determined based on the data only from this study are indicative of a low stress region. The results could be taken as an indication that seismic energy was released in the region during the study period mainly in the form of small magnitude earthquakes. The relatively low b-value estimated by including data from another source shows a relatively high stress for the region. The low b-value estimated by including data from another source may be due to the wide time period considered indicative of the temporal variation of seismicity rate in a given region.

Table of Contents

List of Figures

List of Tables

1. INTRODUCTION

1.1. Background

The Ethiopian rift (ER) system that separates the African (Nubian) plate from the Somalian plate has three major rift parts. These are the Afar Depression, the Main Ethiopian Rift (MER) which forms the third arm of rift-rift-rift triple junction, and the Southern Ethiopian Rift (SER). This seismically and volcanically active rift system has been a target of researchers as it encompasses the various stages of rift development from an early stage of continental break-up to incipient sea-floor spreading in one geodynamic setting. Recent geological and geophysical observations have revealed that the rifting process is localized to the ~ 20 km-wide magmatic segments located along the rift axis (e.g. Mohr, 1967; Bilham *et al.,* 1999; Ebinger and Casey, 2001; Keir *et al.,* 2006a). The major controlling factor of the continental break-up process is the continuous injection of magma into the crust below the along axis magmatic segments (Keranen *et al.,* 2004; Bastow *et al.,* 2005; Keir *et al.,* 2006a). This process has been supported by various tomographic studies and the concentration of seismic activity along this rift floor structures (Keir *et al.,* 2006a). The exact rift extension direction, on the other hand, is unclear. With the majority of results showing rift oblique extension direction (e.g. Boccletti *et al.,* 1998; Bilham *et al.,* 1999; Wolfenden *et al.,* 2004) some studies obtained extension directions orthogonal to the Main Ethiopian Rift (MER) orientation (e.g. McKenzie *et al*., 1970; Chorowicz *et al*., 1994; Korme *et al*., 1997; Acocela and Korme, 2002).

Data from the IRIS/PASSCAL (Incorporated Research Institutes of Seismology/Program for the Array Seismic Studies of the Continental Lithosphere) broadband seismic experiment

(Nyblade and Langston, 2002) is used mainly in this study. In addition, earthquake data from the EAGLE (Ethiopia Afar Geoscientific Lithospheric Experiment) project seismic network and the permanent station FURI are included in the study. The main focus of this work is to assess the seismicity of the region for the period mainly from May to July 2001 and determine other source parameters as well based on the available data.

1.2. Geologic and Tectonic Setting

The Ethiopian Rift (ER) system, which is part of the East African Rift System (EARS) (running for ~6000 km from Mozambique to the Dead Sea), transects the broad Ethiopian plateau of the Afar volcanic province (Fig. 1). It is one of the few areas in the world where ongoing process of continental break-up can be observed on dry land (e.g. Hayward and Ebinger, 1996; Manighetti *et al*., 1997).

Volcanism in the Afar Volcanic Province (also known as the Ethiopia-Yemen flood basalt province) is believed to be initiated by the existence of one or two Paleogene mantle plume(s) underneath (Schilling *et al*., 1992; Ebinger and Sleep, 1998). Geochronological data from Red Sea (RS) rift and Gulf of Aden (GA) show that flood basalt and associated felsic rocks erupted over ~ 1000 km diameter area including the present Afar Depression between 31 and 29 Ma (e.g. Hofmann *et al*., 1997; Ukstins *et al*., 2002). This volcanic activity occurred concurrent with or immediately prior to the initiation of NE-directed extension in the southern RS and GA (Wolfenden *et al*., 2005). ESE-directed extension between the Nubian and Somalian plates commenced in Ethiopia by ca. 18 Ma, and specifically between 18 and 15 Ma in the southern and central Main Ethiopia rift (MER)

(WoldeGabriel *et al*., 1990). On the other hand, in southern Ethiopia rifting took place in a wide zone since 18 – 20 Ma ago (Ebinger *et al*., 2000). Between 12 and 10 Ma, the southern RS margin propagated southward via the Ankober border fault as the MER (which marks the incipient Nubian-Somalian plate boundary) propagated NE via the Arboye border fault (Fig. 1) (Wolfenden *et al.,* 2004) The GA propagated westward into Afar Depression since 16 Ma. This along axis propagation and rifting linked the two rifts and formed the Afar triple junction, also considered as an indication of the onset of extension in the northern MER ca. 11 Ma (more than 17 My after initial rifting in the southern Red Sea and Gulf of Aden) (Wolfenden *et al*., 2004). This chronological relationship led to the conclusion that the flood basalt magmatism and the separation of Arabia from Africa took place widely separated in time from the opening of the MER, making the MER the youngest and least evolved of the three rift arms of the triple junction (Wolfenden *et al*., 2004). Subsequent along axis propagation of rifting in each of the three arms of the triple junction has resulted in a NE-migration of the triple junction since 11 Ma (Wolfenden *et al*., 2004).

The MER, which extends from the southern Afar margin to the Lake Chamo area, is characterized by two main fault systems. These are the $N30^0E$ to $N40^0E$-trending Miocene, steep, segmented border faults, and the Quaternary N-S to $N20^0E$-trending rift floor faults and aligned eruptive centers of the Wonji Fault Belt (WFB) (Mohr 1967; Boccaletti *et al*., 1998). The latter ones began to develop around 1.6 Ma (Meyer *et al*., 1975). The Quaternary faults and associated eruptive centers along the rift floor constitute the youngest part of the MER (Mohr, 1967, 1987; Boccaletti *et al*., 1998, 1999). The northern part of the Southern Ethiopian Rift (SER) is situated west of the southern end of MER, and has a general N-S orientation (Boccaletti *et al*., 1998).

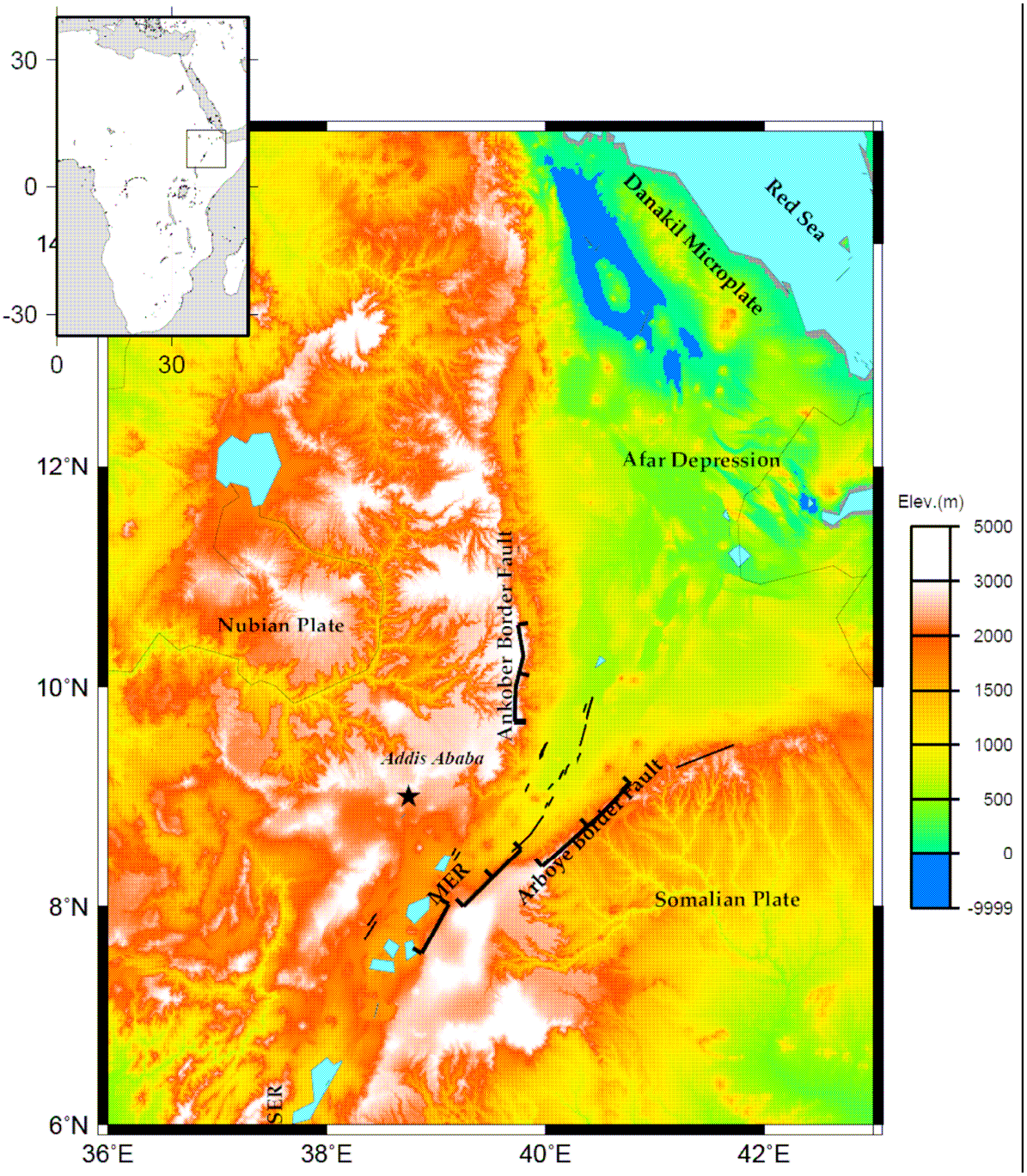

Figure 1. Topographic map of part of Ethiopia showing the major tectonic elements of the rift system. Inset map shows the location of the Ethiopian rift system in Africa. MER represents the Main Ethiopian Rift, SER stands for Southern Ethiopian Rift. Alignment of names in the figure, except those for the two plates and the Afar Depression, coincide roughly with the orientations of the rift structures they are meant to represent. Solid lines are faults.

The rift system shows crustal thickness variations both along the axis and across the rift. Along the MER axis a decrease in crustal thickness from *c*. 38 km in the south around the lakes region to 26 km beneath the northeastern end of the MER is estimated (Dugda *et al*., 2005; Maguire *et al*., 2006). Results from seismic reflection/refraction data and receiver function analysis show 38 – 40 km-thick crust beneath the southeastern plateau, whereas the western side of the rift is underlain by 45-50 km-thick crust with ~10-15 km high velocity lower crust (Mackenzie *et al*., 2005; Stuart *et al*., 2006; Maguire *et al*., 2006). This low velocity layer was interpreted as an underplate (Mackenzie *et al*., 2005) associated with Oligocene flood basalt and recent magmatic activity (Mackenzie *et al*., 2005; Maguire *et al*., 2006) or remnant of dynamic uplift (Tiberi *et al*., 2004). The MER is also characterized by segmented along axis upper-mantle low velocity zones and high velocity elongated and cooled crustal mafic intrusions beneath the rift attributed to the anomalous hot upper mantle and local melt ponds (Keranen *et al.,* 2004; Bastow *et al.,* 2005). According to Bastow *et al*., (2005), the distribution and extent of these segments is indicative of the increasing degrees of extension and magmatic intrusion as one moves from south to north in to the Afar Depression. The Afar Depression has a crustal thickness of 20 – 25 km and thins to 16 km in the north (e.g. Dugda *et al*., 2005; Garfunkel and Beyth, 2006).

A change from 130^0 E-directed extension to 105^0 E-directed extension in the interval from 6.6 to 3 Ma is revealed by structural patterns (Boccaletti *et al*., 1998; Wolfenden *et al*., 2004). Chu and Gordon (1999) estimated the Nubian-Somalian separation since 3.2 Ma ago to be > 5 mm/yr across the northern MER, and ~16 mm/yr between Africa and Arabia across the Afar Depression. Bilham *et al*., (1999) from geodetic measurements obtained for the NNE-trending MER an opening rate of 4.5±1.0 mm/yr and extension direction of

108^0E±10^0. The elliptical shape of the active volcanoes of Fantale, Boset and Dofen which have their major axis in the direction of plate motion led Ebinger and Casey (2001) and Casey *et al*. (2006) to infer Holocene rift extension direction of N105^0 E. In contrast, Acocella and Korme (2002), from field analysis of extensional fractures along the axis of the MER, determined a mean Holocene extension direction of N52^0W±20. This perpendicular extension direction to the MER, although oblique to the active fractures in the rift, was considered in their work as an indication of the kinematics between the Nubian and Somalian plates in Ethiopia.

Geodetic data shows that present-day extension within the northern MER has localized to < 20 km-wide zones of aligned volcanoes and associated flows (Bilham *et al*., 1999). This result is in agreement with other observations that supported the fact that the locus of extension and magmatism migrated or jumped to the narrow magmatic segments in the past 2 Ma (Ebinger and Casey, 2001; Wolfenden *et al*., 2004). It is also revealed that these magmatic segments accommodate > 80 % of the strain across the rift, supportive of the fact that border faults are not the major locus of extension (Bilham *et al*., 1999; Ebinger and Casey, 2001). The Quaternary magmatic segments are narrow, right-stepping en echelon fault zones and magmatic centers within the central rift valley (Ebinger and Casey 2001). Volcanism in the magmatic segments commenced ca. 1.6 Ma; most flows emanated from fissures or small cinder cones (WoldeGabriel *et al*., 1990; Boccaletti *et al*., 1999; Ebinger and Casey, 2001). Models of gravity and geodetic data suggest that the narrow magmatic segments are underlain by mafic intrusions (Bilham *et al*., 1999; Mahatsente *et al*., 1999) interpreted as a zone of intensive dike injection. Keranen *et al*., (2004) from studies of crustal tomographic structure of the MER interpreted the high velocity bodies underlying the

Quaternary magmatic segments as cooled mafic intrusions. Based on the above evidences and others, Keir *et al*., 2006a concluded the intrusion of magma beneath the ~ 20 km-wide magmatic segments controls the majority of straining, seismicity and faulting during continental break-up.

1.3. Previous Seismotectonic Studies

It is believed that seismic activity associated with the rift development has been there for longer time in Ethiopia than the instrumentally and historically recorded data. The lack of earthquake recording instruments in the early days of earthquake occurrence and sparse distribution afterwards made the earthquake catalogue for the region incomplete. Documented observations about the historic earthquakes for over 500 years in Ethiopia were collected from various sources and compiled by Gouin (1979). The distribution of these events shows that the Afar Depression and the western margin of the northern ER have a long history of seismic activity. In the monograph of Gouin (1979), the maximum magnitude of events observed in the whole region considered is 6.8. Some of the largest events are discussed in brief below. The August 25, 1906 earthquake with magnitude 6.8 (M_s) in the Langano area, which was also felt in Addis Ababa and its surroundings, is one of the reported events. This event is relocated by Ayele and Kulhanek (2000) to the eastern shoulder of the Ethiopian rift with M_w=6.5. An earthquake swarm was also reported in 1961 near Kara Kore which caused damage to man-made structures (completely destroyed the town of Majete) and alterations in the landscape – the maximum magnitude was greater than 6.4. The other major event in the report is the May - March 1969 Serdo (in the central Afar

Depression) earthquake sequence. The main shock had a magnitude M_b=5.9 that destroyed completely the town of Serdo with some casualties.

Earthquake catalogue of the Horn of Africa is also compiled for the period from 1960 – 1993 with a threshold magnitude of 4.5 (m_b) by Ayele (1995). This catalogue shows relatively high seismicity, considering the Ethiopian part only, in the Afar Depression and northern part of the western rift margin. In agreement with the localization of deformation to the magmatic segments (Bilham *et al*., 1999; Ebinger and Casey, 2001; Hofstetter and Beyth, 2003; Wolfenden *et al.,* 2004), the epicenteral distribution for the MER for the period from October 2001 to January 2003 (Keir *et al.,* 2006a) shows coincidence with these active centers. The only exception was the seismicity observed along the Ankober border fault. An increase in focal depth is observed as one goes from north to south along the rift system. These focal depth variation together with the low stress drop obtained for the Afar region was taken to infer the presence of soft material at a shallower depth in Afar and neighboring regions (Kebede, 1989; Kebede *et al*., 1989).

Source mechanism studies have been done for a number of earthquakes in the ER (e.g. Kebede, 1989; Kebede *et al.,* 1989; Ayele and Arvidsson, 1998; Ayele, 2000; Keir *et al.,* 2006a, Ayele *et al.,* 2007, Fig. 2), though small compared to the total seismicity of the region. Based on earthquake data from the East African Rift System (EARS) as a whole and central and western margin of Afar Depression in particular, Kebede (1989) and Kebede *et al*., (1989) determined normal fault mechanisms and interpreted as an implication of the extensional tectonics in EAR. P-wave first motion analysis for the largest four earthquakes from the 1969 May - March central Afar earthquake sequence resulted in fault plane

solutions showing predominantly strike-slip faulting (Kebede *et al.,* 1989). According to these authors, these strike slip solutions are taken as confirmation for the presence of transform fault in Afar. In the southern part of ER, where the monitoring of seismicity is relatively low, two sets (in terms of distribution and to some extent solutions) of source mechanisms were obtained. The solutions for the earthquakes from southwestern Ethiopia show dominantly normal faulting with the fault planes trending in the direction of the MER (Ayele and Arvidsson, 1998). This fault plane orientation was considered as a manifestation of the continuation of the mode of deformation of the MER southward despite morphological discontinuity. Ayele (2000) determined fault plane solutions for four earthquakes from the eastern side of MER. The results show normal faulting with significant left-lateral strike-slip components – manifestation of the existence of sinistral oblique deformation between the Somalian plate and the Nubian plate. In addition to the aforementioned types of source mechanisms, normal faulting solutions with roughly N-S extension directions are reported in Gewane and Afar Depression (Ayele *et al.,* 2006, and references therein).

As an integral part of the seismicity study of the EARS and its parts, researchers have determined different b-values. Kebede and Kulhanek (1991 and 1994) determined b-values of 0.5-0.8 for the Afar Depression and neighboring regions. The estimates of b-values obtained using information in (Ayele, 1995) are in the range from 0.5 to 1.1 for the northeastern part of the ER. Lower b-values are for the continental parts (Ayele and Kulhanek, 1997). This result is in agreement with the b-value of 0.67±0.16 calculated for the August 2002 swarm (Ayele *et al.,* 2007). Keir *et al.,* (2006b) using data from EAGLE calculated a b-value of 1.13±0.05 for the MER alone, and Hofstetter and Beyth (2003)

estimated a b-value of 0.83±0.08 from 16 earthquakes obtained from global and regional catalogues that were located over a wide region in MER and southern Ethiopia.

1.4. Objectives and Significance of the Study

Continuous monitoring of seismicity is crucial to determine and understand the various processes modifying the rift systems. The lack of sufficient earthquake recording stations has been a major problem in the study of seismicity of the country. This resulted in an incomplete earthquake catalogue of the region. The current work presents an earthquake catalogue for the study period and attempts to determine other earthquake related parameters. The following are considered as the primary aims of this paper:

1 - To provide a complete earthquake catalogue of Ethiopia for the period from May to July 2001 determined with high accuracy,

2 - Estimate local magnitude of the located earthquakes using the recently developed scale for the MER by Keir *et al.,* (2006b),

3 - Determine source mechanisms for selected earthquakes from the catalogue

4 - Estimate b-values for the whole region where the epicenters are distributed and for the high seismicity area during the study period by including data from other source.

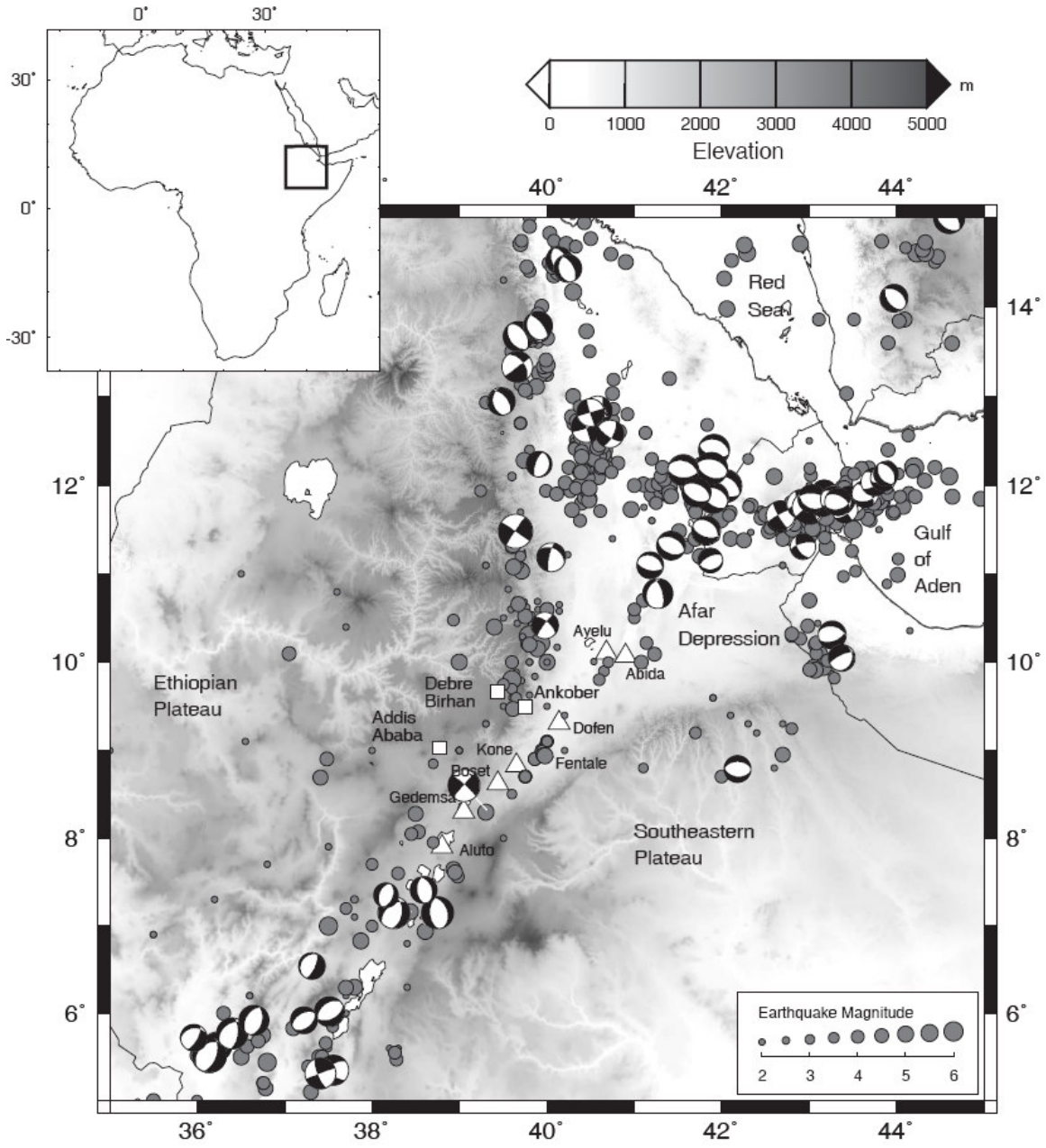

Figure 2. Seismic activity of the Horn of Africa since 1960-2003 (after Keir *et al.,* 2006a). Gray circles are earthquake epicenters and white triangles show locations of Quaternary volcanoes. The square in the inset shows the region for which epicenters and focal mechanisms are plotted.

The determination of the above seismic parameters will have significant importance in understanding the ongoing rifting process. The complete catalogue of hypocentral parameters can be taken as an input for further seismological works such as regional and local seismotectonic studies apart from documenting the distribution of seismic activity in time and space. The majority of source mechanisms determined for the earthquakes in the region are either based on data obtained from global and regional networks or for the largest earthquakes only. These results, though, helpful in understanding the overall kinematics of the rift system, may not necessarily show small-scale tectonic features. The fault plane solutions determined for the relatively small magnitude earthquakes obtained from local network, therefore, could possibly show the local tectonics of their respective regions. For seismic hazard analysis of a region reliable estimates of the b-value is vital. Therefore, the estimates of this study can also be used in the hazard assessment of the areas for which b-values are determined.

2. SEISMIC WAVE PROPAGATION – THEORY

Seismology is the science of earthquakes which are generated as a result of transient stress imbalances in the interior of the earth. During an earthquake seismic (elastic) waves are generated and seismology studies the origin (source nature) of these waves, their propagation through the Earth's interior, and their recording and interpretation. In other words, seismology directly focuses on the analysis of ground motions recorded at some distance from the source of the disturbance. The sources of these disturbances can be natural such as earthquake faulting or man-made causes like explosions. When there is a stress imbalance, deformation/strain result which in turn generates seismic waves. Therefore, the key problem in seismology is the study of the relation between the deforming forces in a medium and the resulting deformation.

To fully describe and interpret a seismic record which is the result of the combined effects of the source, propagation path and recording instrument, understanding of the basics of wave propagation theory is necessary. In the following sub-sections the basic theories are discussed briefly.

2.1 The Theory of Elasticity

An earthquake occurs in the earth's interior (crust and upper mantle) when the tectonic stress (deformational force applied per unit area) exceeds the local strength of the rocks and failure occurs. The resulting seismic (elastic) waves propagate away from the source region by elastic deformation of the rocks through which they travel. Therefore, their propagation

depends on the elastic properties. The theory of elasticity provides mathematical relationships between the forces applied on a medium (stresses) and the resulting deformations (strains). The relation between stress and strain is used to describe the elastic properties of a medium. It is given by the generalized form of Hook's law as:

$$\sigma_{ij} = C_{ijkl}\varepsilon_{kl}, \qquad (1)$$

where σ_{ij} is the stress tensor, C_{ijkl} represent the constants of proportionality known as elastic moduli and ε_{kl} is the strain tensor.

2.2 The Strain Tensor

Deformations in a medium are divided as those that involve length changes and those that involve angular distortions. The former ones result in elongation of the medium and are defined as normal strains. The normal strains (Fig. 3) are given by

$$\varepsilon_{normal} = \left(\frac{L + \Delta L - L}{L}\right), \qquad (2)$$

where $L + \Delta L$ is the length after deformation

L is the original length

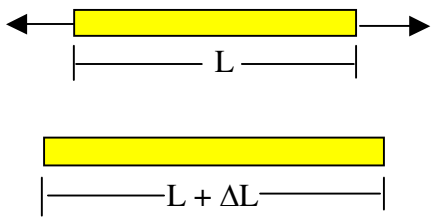

Figure 3. Sketch of normal straining involving changes in length. Force is applied on both sides as shown by the arrows.

The angular distortion (Fig. 4) in a medium is described as shear strain and is given by

$$\varepsilon_{shear} = \frac{1}{2}\left(\frac{\pi}{2} - \theta\right), \tag{3}$$

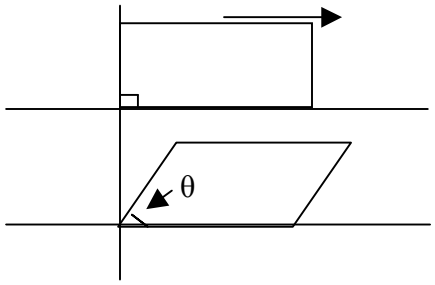

Figure 4. Sketch of shear straining involving angular distortion. The base of original rectangle is assumed to be fixed and force is applied as shown by the arrow.

where θ is the angle between two line segments that were perpendicular before deformation. Considering a three-dimensional coordinate system, the full description of strain in a medium will have three normal strains and six shear strains. The three normal strains describe length changes in the coordinate directions and the six shear strain components give angular changes of each coordinate direction with respect to the other two directions. By defining a displacement vector **u(x, t)** of each point in a medium in a Cartesian coordinate system and making use of the description in (2) and (3), the strain-displacement relationships can be derived (Lay and Wallace 1995). The full components of infinitesimal strain tensor (ε_{ij}) in terms of displacements (Aki and Richards 1980; Lay and Wallace 1995) is, therefore, given as

$$\varepsilon_{ij} = \begin{pmatrix} \varepsilon_{11} & \varepsilon_{12} & \varepsilon_{13} \\ \varepsilon_{21} & \varepsilon_{22} & \varepsilon_{23} \\ \varepsilon_{31} & \varepsilon_{32} & \varepsilon_{33} \end{pmatrix}$$

$$= \begin{pmatrix} \dfrac{\partial u_1}{\partial x_1} & \dfrac{1}{2}\left(\dfrac{\partial u_2}{\partial x_1} + \dfrac{\partial u_1}{\partial x_2}\right) & \dfrac{1}{2}\left(\dfrac{\partial u_1}{\partial x_3} + \dfrac{\partial u_3}{\partial x_1}\right) \\ \dfrac{1}{2}\left(\dfrac{\partial u_2}{\partial x_1} + \dfrac{\partial u_1}{\partial x_2}\right) & \dfrac{\partial u_2}{\partial x_2} & \dfrac{1}{2}\left(\dfrac{\partial u_2}{\partial x_3} + \dfrac{\partial u_3}{\partial x_2}\right) \\ \dfrac{1}{2}\left(\dfrac{\partial u_1}{\partial x_3} + \dfrac{\partial u_3}{\partial x_1}\right) & \dfrac{1}{2}\left(\dfrac{\partial u_2}{\partial x_3} + \dfrac{\partial u_3}{\partial x_2}\right) & \dfrac{\partial u_3}{\partial x_3} \end{pmatrix}, \qquad (4)$$

where the ε_{ii}'s are the normal strains and the off-diagonal elements are the shear strains, $u_{i,j} = \dfrac{\partial u_i}{\partial x_j}$ and the u_is are the displacements in the i^{th} coordinate direction.. The first subscript indicates the orientation of the fixed line segment and the second indicates the orientation of the deforming segment. In compact indicial notation eq. (4) is written as

$$\varepsilon_{ij} = \frac{1}{2}(u_{i,j} + u_{j,i}), \qquad (5)$$

2.3 The Stress Tensor

The stresses, which is the force exerted per unit area, in a medium are also expressed as normal and shearing stresses. The normal stresses are due to the force acting normal to the surface considered, while shear stresses are associated with forces tangential to the surface. Accordingly there are nine stress components; three normal-stress components which are

perpendicular to the coordinate planes, and six tangential stress components acting tangent to the coordinate planes (Fig. 5). The stress tensor σ_{ij} is given by

$$\sigma_{ij} = \lim_{\Delta A_i \to 0} \frac{\Delta F_j}{\Delta A_i}, \qquad (6)$$

where i corresponds to the direction of the normal to the plane being acted on by the force F, and j corresponds to the direction of the applied force. On any arbitrarily oriented surface th-

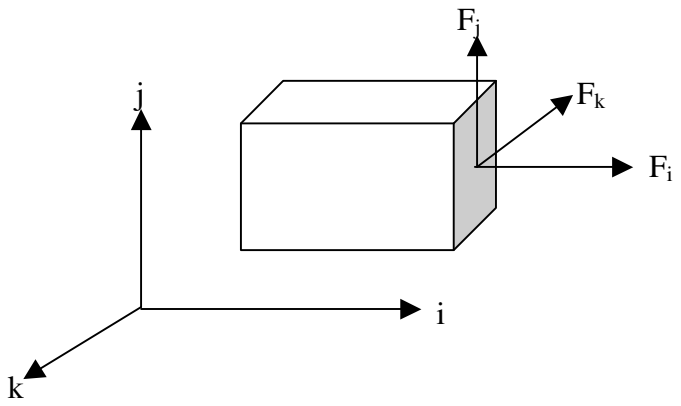

Figure 5. Sketch with one face (shaded) of a cub acted upon by normal (F_i) and tangential (F_j and F_k) forces. The relationship between the direction of these forces and area represented by its normal determines the component of the stress tensor.

rough the medium the stress vector or traction vector T_i is determined by assuming state of equilibrium (Aki and Richards 1980; Lay and Wallace 1995). The fact that for a body to be in equilibrium the sum of all forces and moments must be zero results in the general representation of Traction vector as

$$T_i = \sigma_{ij}\, n_j, \qquad (7)$$

where n is the normal to the arbitrary surface considered. The traction vector or stress vector is used to analyze the internal forces acting mutually between adjacent particles within a continuum.

In matrix form the stress tensor is written as:

$$\sigma_{ij} = \begin{pmatrix} \sigma_{11} & \sigma_{12} & \sigma_{13} \\ \sigma_{21} & \sigma_{22} & \sigma_{23} \\ \sigma_{31} & \sigma_{32} & \sigma_{33} \end{pmatrix}, \qquad (8)$$

The diagonal elements are the normal stresses and the off-diagonal terms are the shear stresses. Normal stresses with positive values (directed outward from the body) are called tensional stresses and those with negative values are called compressional stresses.

The C_{ijkl} term in eq. (1) has 81 terms for the general form relating the nine elements of the strain tensor to the nine elements of the stress tensor. Applying the symmetric natures of the stress and strain tensors and further assuming homogenous, isotropic and linearly elastic medium, the number of elastic constants can be reduced to only two. These constants are known as the *Lame constants*, λ and μ, and they are related to C_{ijkl} by

$$C_{ijkl} = \lambda\delta_{ij}\delta_{kl} + \mu(\delta_{ik}\delta_{jl} + \delta_{il}\delta_{jk}), \qquad (9)$$

where δ is the Kronecker delta function. Substituting eq. (9) into eq. (1) gives

$$\sigma_{ij} = [\lambda\delta_{ij}\delta_{kl} + \mu(\delta_{ik}\delta_{jl} + \delta_{il}\delta_{jk})]\varepsilon_{kl} \qquad (10)$$

which reduces to

$$\sigma_{ij} = \lambda\theta\delta_{ij} + 2\mu\varepsilon_{ij}, \qquad (11)$$

where $\theta = \frac{\partial u_1}{\partial x_1} + \frac{\partial u_2}{\partial x_2} + \frac{\partial u_3}{\partial x_3}$

δ_{ij} is the Kronecker delta function given by

$$\delta_{ij} = \begin{cases} 1 \; for i = j \\ 0 \; for i \neq j \end{cases} \quad i, j = 1, 2, 3$$

λ and μ are Lamé constants (μ is shear modulus – a measure of resistance to shearing)

2.4 The Equation of motion

The propagation of the elastic disturbance which resulted from the stress imbalance in a medium can be mathematically represented using the above equations of stress, strain and the generalized form of Hook's law. Taking into account the effects of body forces in a medium and applying Newton's 2nd law, the equation of motion is given by the general form as

$$\rho \frac{\partial^2 u_i}{\partial t^2} = f_i + \frac{\partial \sigma_{ij}}{\partial x_i}, \qquad (12)$$

where ρ is density of the material and f is the body force per unit volume. Since the body forces such as gravitational forces do not vary much with distance (Aki and Richards 1980), the homogenous equation of motion is given by neglecting the body force terms from (12) as

$$\rho \frac{\partial^2 u_i}{\partial t^2} = \frac{\partial \sigma_{ij}}{\partial x_i} \qquad (13)$$

Substituting (5) and (11) into (13), we can write the three-dimensional vector equation of motion for a homogenous, isotropic, linear elastic medium as

$$\rho \frac{\partial^2 \vec{u}}{\partial t^2} = (\lambda + \mu)\vec{\nabla}\left(\vec{\nabla} \cdot \vec{u}\right) + \mu \vec{\nabla}^2 \vec{u}, \qquad (14)$$

where ∇ is the 'del' operator and ∇^2 is the Laplacian operator. Using the vector identity

$$\vec{\nabla}^2 \vec{u} = \left(\vec{\nabla} \cdot \vec{u}\right) - \left(\vec{\nabla} \times \vec{\nabla} \times \vec{u}\right) \qquad (15)$$

an alternative form of (14) is given by

$$\rho \frac{\partial^2 \vec{u}}{\partial t^2} = (\lambda + 2\mu)\vec{\nabla}\left(\vec{\nabla} \cdot \vec{u}\right) - (\mu \vec{\nabla} \times \vec{\nabla} \times \vec{u}) \qquad (16)$$

Equation (14) and (16) are of the form Force = mass X acceleration in terms of particle displacements for a general deformation transmitted through a homogeneous, isotropic, linearly elastic medium. The equations are based mainly on the assumptions of infinitesimal strain and no body forces.

The equation of motion (16) can be solved by applying the Helmholtz's theorem (Aki and Richards 1980; Lay and Wallace 1995). According to the Helmholtz's theorem, any vector field **u** (**x, t**) can be represented in terms of a divergenceless vector potential **ψ** and a scalar potential **Φ** that involves no rotational deformation as

$$\mathbf{u} = \vec{\nabla}\Phi + \vec{\nabla}\times\boldsymbol{\psi}, \qquad (17)$$

where $\vec{\nabla}\times\Phi = 0$ (Φ is curl free)

$\vec{\nabla}\cdot\boldsymbol{\psi} = 0$ ($\boldsymbol{\psi}$ is divergence free)

Therefore, if **u**(**x, t**) satisfies the equation of motion and is represented according to (17), substituting eq. (17) and using the vector identity ($\vec{\nabla}\times\vec{\nabla}\times\vec{\psi} = -\vec{\nabla}^2\vec{\psi}$ since $\vec{\nabla}\cdot\boldsymbol{\psi} = 0$), gives

$$\vec{\nabla}[(\lambda+2\mu)\vec{\nabla}^2\phi - \rho\frac{\partial^2\phi}{\partial t^2}] + \vec{\nabla}\times[\mu\vec{\nabla}^2\vec{\psi} - \rho\frac{\partial^2\vec{\psi}}{\partial t^2}] = 0 \qquad (18)$$

The following equations hold true (Aki and Richards 1980) if eq. (18) is satisfied when each term in the brackets goes to zero independently:

$$\frac{\partial^2 \phi}{\partial t^2} = \alpha^2 \vec{\nabla}^2 \phi, \qquad (19), \text{ and}$$

$$\frac{\partial^2 \vec{\psi}}{\partial t^2} = \beta^2 \vec{\nabla}^2 \vec{\psi}, \qquad (20)$$

with

$$\alpha^2 = \frac{\lambda + 2\mu}{\rho} \quad \text{and} \quad \beta^2 = \frac{\mu}{\rho}$$

The $\vec{\nabla}\phi$ and $\vec{\nabla} \times \boldsymbol{\psi}$ are called the P-wave and S-wave components of the displacement vector **u**. This result shows the displacement field created by a stress imbalance is completely accounted for by propagating P and S waves for any given source type (Aki and Richards 1980; Lay and Wallace 1995). These wavefields become increasingly complex when discontinuous material properties and localized inhomogeneities are present resulting in the formation of Surface waves.

3. DATA AND METHODOLOGY

3.1. Data Sources

Data obtained from the IRIS/PASSCAL seismic experiment in Ethiopia (Nyblade and Langston 2002) was used primarily in this study. This experiment was operational between 2000 and 2002. The twenty-six three component broadband seismic stations of this experiment were distributed in the country (Fig. 6) covering an area of 500 x 500 km.

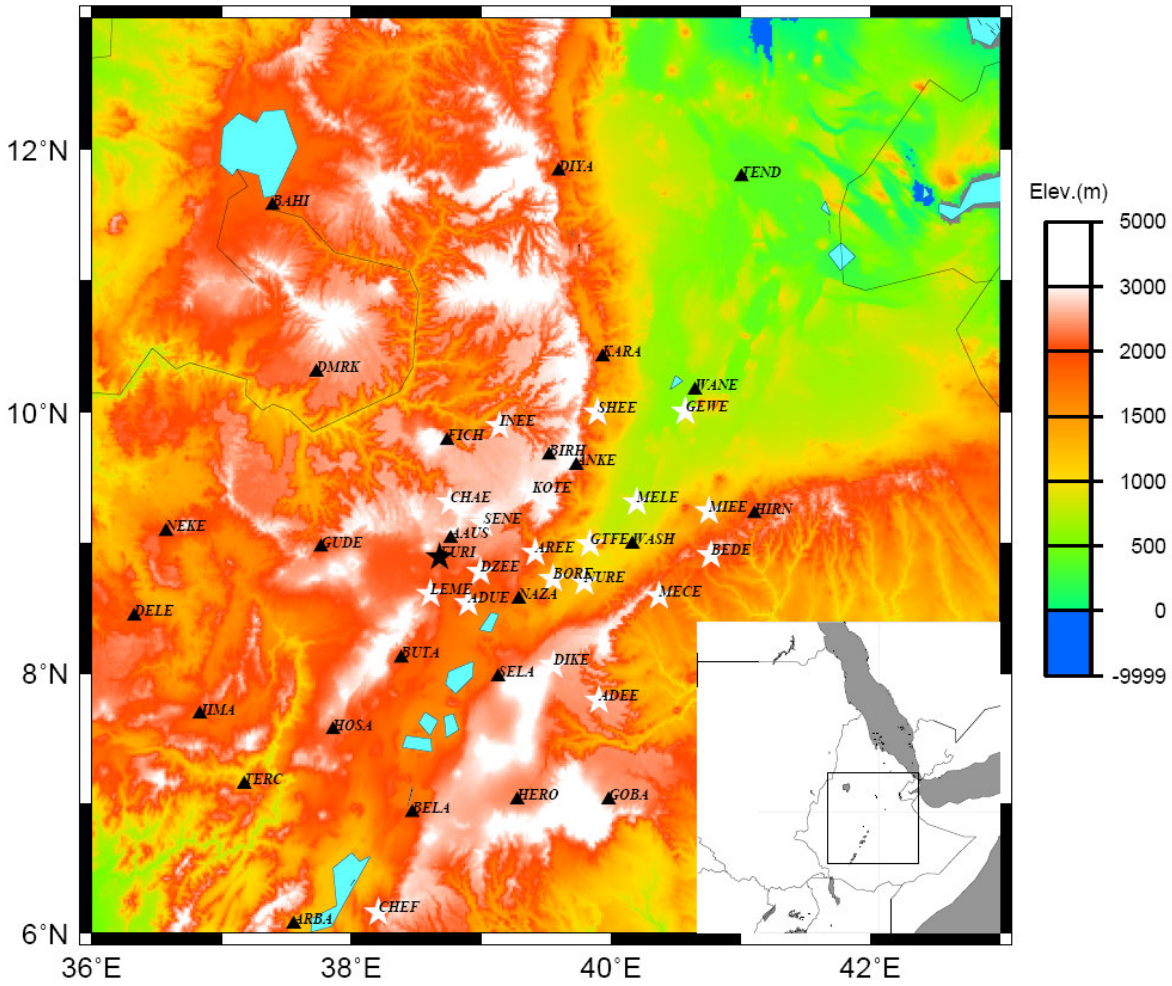

Figure 6. Distribution of earthquake recording stations used in this study. Black triangles mark the locations of the IRIS/PASSCAL experiment stations. White stars mark the EAGLE stations. Black star represents the location of the permanent station FURI.

In addition, data from twenty-one broadband stations of the EAGLE network and from the permanent broadband station FURI were included in the determination of earthquake locations and other related parameters.

3.2. Methodology

3.2.1. Seismic Phase Picking

Appropriate programs are used to make the data obtained from the IRIS/PASSCAL seismic experiment stations ready for plotting using SAC (Seismic Analysis Code) (Fig. 7). This plotting and analysis software was also used to plot data from FURI and EAGLE stations. P- and S- first arrival times were picked from vertical and horizontal components, respectively (Fig. 8). In cases where the noise level for the records is higher various filters were applied to determine the arrival times with better accuracy. Arrival times were read for all earthquakes, regardless of their size and source region, recorded by the stations for months May, June and July. For the following months of 2001, arrivals were picked for selected earthquakes based on their size.

3.2.2. Earthquake Location Methods and Programs

For the determination of hypocentral locations phase reading data (mostly of P-wave arrivals), station locations, a well-constrained 1-D velocity model determined from EAGLE (Daly *et al.,* 2004) (Table 1) and a Vp/Vs ratio of 1.75 were used. According to the quality of the readings, the P-wave arrivals were assigned weights of 1 (full), 0.75, 0.5 and 0.25. Those earthquakes that were recorded by at

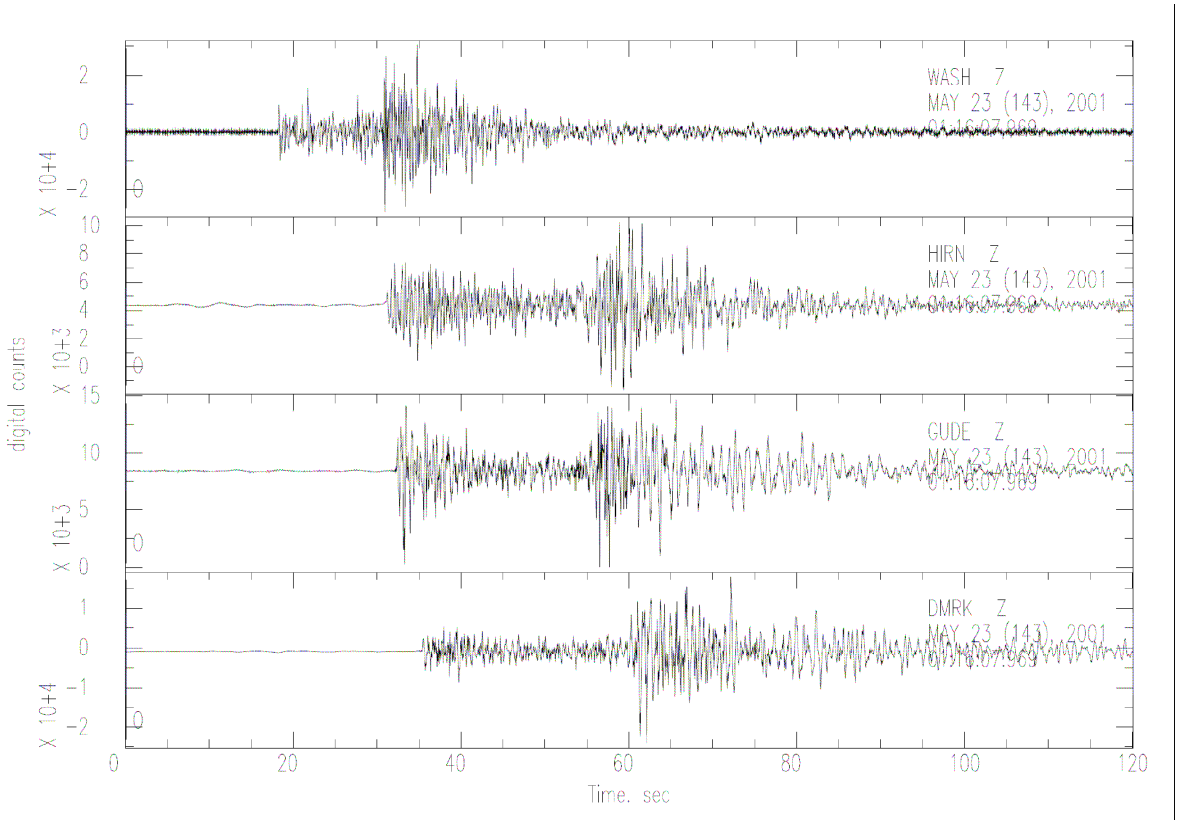

Figure 7. Unfiltered vertical component recordings of an earthquake on 23/05/2001 located near Ankober from the stations WASH, HIRN, GUDE and DMRK, and plotted using the SAC program.

least four stations were used in the location process and only the local earthquakes were used for subsequent analysis. The location programs (Hypoincerse2000 and HypoDD) follow the principles of inverse theory based on arrival time data of the different phases and the station locations. That is, for a given earthquake the programs assign values first for the hypocenter parameters (x, y, z, t_o) and use information about the seismic station locations (x_i, y_i, z_i) and arrival times (t_i). The x's, y's and z's are corresponding location parameters, and t_o and t_i are origin time and arrival times (Lay and Wallace 1995; Menke 1987).

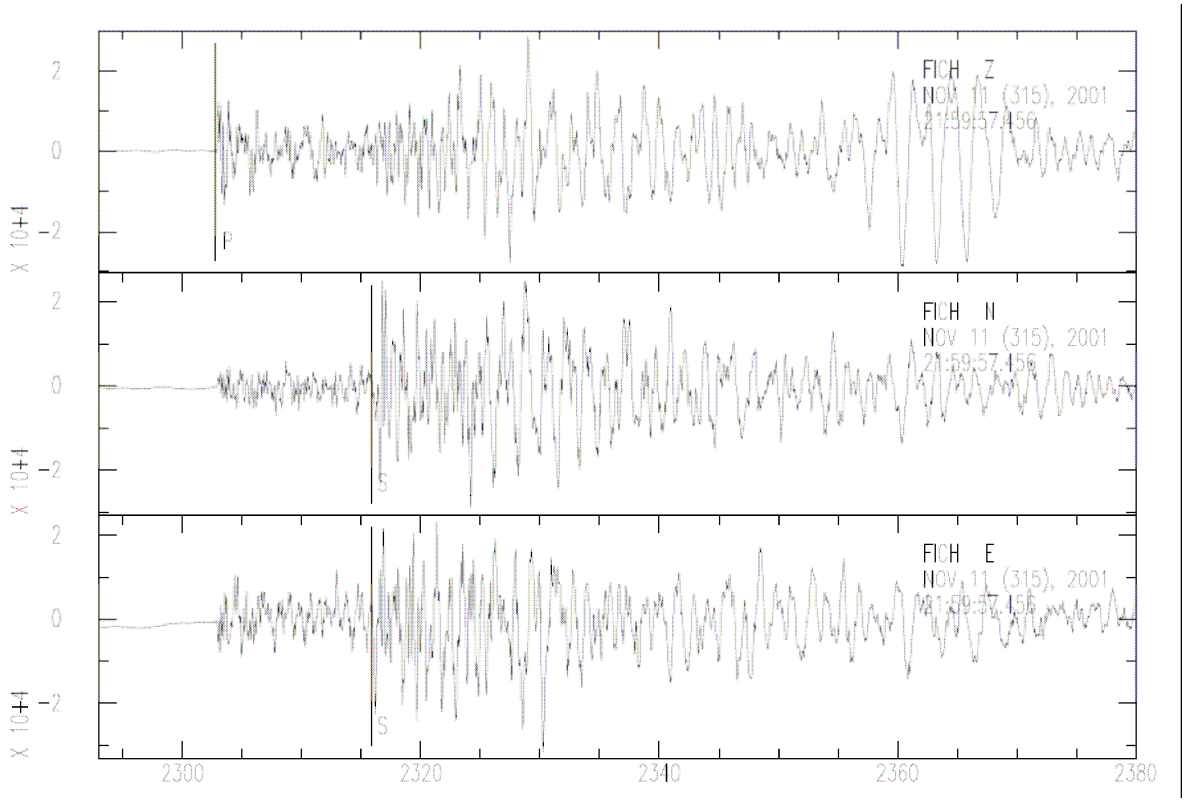

Figure 8. Sample SAC plot for an earthquake recorded at FICH. P- and S-picks are also shown on the plot. The earthquake occurred on 11/11/2001 near Ankober with local magnitude of 3.9.

Table 1. Velocity model used for earthquake location (from Daly *et al*., 2004)

Depth (km)	0.0	2.0	3.0	5.0	11.0	23.0	40.0
V_P (km/s)	3.03	3.30	5.54	5.61	6.22	6.7	7.5

For each station the input files are combined as follows:

$$t_i = t_o + \frac{\sqrt{(x_i - x)^2 + (y_i - y)^2 + (z_i - z)^2}}{V}, \qquad (19)$$

where - V is velocity in km/s

i is the i^{th} station

When computed for all the arrival times at each station, the above equation gives a system of equations This way the t_i's form the data vector **d** of n-dimension/observations, and x, y, z, and t_o make elements of the model vector **m** of m-dimensions (four in this case). The system of equation is, therefore, written as

$$\mathbf{F}\ (x, y, z, t_o) = \mathbf{d} \qquad (20)$$

Eq. (20) is a non-linear function, which is characteristic of earthquake location problem. The standard procedure is to linearize the problem and iteratively determine the model parameters that best fit to the observed data. The linearization process through the use of Taylor series expansion of Eq. (20) results in a system of linear equations that relate the model parameters to the observed data (Menke, 1987). The resulting equation is given as

$$\mathbf{d = Gm}, \qquad (21)$$

where G is the data kernel

Since the determination of hypocenter in this study has a minimum of four elements of **d**, it is an overdetermined problem, and has no exact solution. The best-fit solution is obtained by iteratively minimizing the residual/difference between observed and predicted data in the least squares sense. The least-squares solution for the hypocentral parameters is determined as follows

$$\mathbf{m} = [\mathbf{G}^T\mathbf{G}]^{-1}\mathbf{G}^T\mathbf{d} \qquad (22)$$

The natural solution of (21) can also be solved using the method of singular value decomposition. It is written as

$$\mathbf{m} = \mathbf{V_p}\mathbf{\Lambda_p}\mathbf{U_p}^{-1}\mathbf{d}, \qquad (\mathbf{23})$$

where p - number of non-zero eigen values

V_p - the first p columns of the eigen vector spanning the space of all model parameters

$\mathbf{\Lambda_p}$ – a p x p diagonal matrix of non-zero eigen values

U_p - the first p columns of the eigen vector spanning the space of all possible data

The decomposition of G is given by

$$\mathbf{G} = \mathbf{U}\Lambda\mathbf{V}^T \qquad (24)$$

The corresponding eigen values and vectors are determined by solving the characteristics polynomial equations obtained from the following relations:

$$\mathbf{GV = \Lambda U,\ G^T U = \Lambda V,\ G^T G V = \Lambda^2 V,\ G G^T U = \Lambda^2 U} \qquad (25)$$

3.2.2.1. Hypoinverse-2000

Hypoinverse-2000 (Klein 2002) is one of the two location programs used in the determination of hypocentral parameters in this study. It uses the method of singular value decomposition and successive iterations in linear steps until a solution that best fits the observations is obtained. Parameters that control the location process are fed either as an input file or from the command prompt line. Among these, the major ones are phase arrival time, station location file and velocity model files. The RMS (root-mean-square) travel time residual between observed and predicted travel times) is calculated using the formula

$$RMS = \frac{\sum_{i=1}^{n} (w_i r_i)^2}{\sum_{i=1}^{n} w_i^2}, \qquad (26)$$

where $r_i = t^{observed} - t^{preditced}$, and

w_i = weight of individual residuals

3.2.2.2. HypoDD

The second location program used here is HypoDD. It is a program for relocating earthquakes with the double-difference algorithm of Waldhauser and Ellsworth (2002). The program package is widely used mainly because it provides an efficient method to determine high-resolution hypocentral locations by inverting for relative locations within a cluster. This relocation process takes earthquake locations as input that were located individually with single event programs such as Hypoinverse-2000. In addition, an a priori velocity model is required.

To determine the location with high accuracy, the algorithm requires the hypocentral separation between two earthquakes to be small compared to the event-station distance, and assumes the ray paths between the source region and a common recording station are similar along the entire path. In this case, the difference in travel times for the two events recorded at a given station is attributed to the spatial offset between the events with high accuracy and the program tries to remove the effects due to this un-modeled velocity structure. The double-difference algorithm attempts to minimize the residual between observed and calculated travel-time difference (double-difference) for a pair of earthquakes at a single station. The event pairs are defined by parameters set either as control files or from the prompt line. In this study, the method of singular value decomposition is implemented as it is recommended for a problem with small number of earthquakes.

3.2.3. Magnitude Determination

The first step in the determination of earthquakes magnitude in this study was to read amplitude. For an earthquake, waveforms from two or more stations that have good quality N-S and E-W component records were selected. These waveforms were then corrected for the instrument responses of the seismometers used at the respective stations. The resulting displacement ground motions were convolved with the standard Wood-Anderson response using the SAC program. The wood-Anderson filter has a magnification of 2800, damping ratio of 0.8, and natural period of 0.8 sec. (Anderson and Wood, 1925). Maximum peak-to-peak amplitude in mm was measured and halved to obtain the zero-to-peak amplitude value to be used later in the determination of local magnitude, ML.

The local magnitude scale determined by Keir *et al.,* (2006b) is used here. It is given as

$$\mathbf{M_L = \log(A_{WA}) - \log(A_O) + C,} \qquad (27)$$

where A_{WA} is zero-to-peak amplitude measured on a standard Wood-Anderson seismogram, $\log(A_O)$ is a distance correction term and C is the correction term for individual stations. The distance correction term was estimated by Keir *et al.,* (2006b) to be

$$\log(A_O) = -1.196997 * \log(r/17) - 0.001066 * (r - 17) - 2, \qquad (28)$$

where r is the hypocentral distance in Kilometers.

The determination of magnitude for a given earthquake was done in three-step (Appendix A). First, M_L was determined for each horizontal component at a given station using the corresponding amplitude data and the above magnitude scale. The average of these two magnitude estimates was then computed. Finally, to reduce the effect of C, which is influenced more by local site effects Keir *et al.,* (2006b), M_L was calculated at two and more stations by considering the closest and farthest stations and the values were averaged out.

3.2.4. Determination of Fault Plane Solutions

Fault plane solutions were computed from P-wave polarities using the SEISAN (Havskov and Ottemoller, 2000) version of grid search algorithm of Snoke *et al.,* (1984). Hypocentral locations from the Hypoinverse program were used. The major selection criterion was the minimum number of polarity readings, which was 10, and good station azimuthal coverage.

The basic assumption considered in the estimation of fault plane solution is that the polarity of the P-wave displacements will be preserved along the associated path to any receiver because the wave transmits the initial motion from particle to particle without modification (Lay and Wallace, 1995). The convenient approach to visualize the three dimensional characteristics of the seismic wave radiations from the source that were recorded at various stations in the form of P-wave polarities is to imagine a focal sphere around the source. By applying the above assumption a ray can be traced back to its source. The two parameters that are required to trace a ray back are the azimuth (θ) and takeoff angle (i) which can be calculated from the source-station orientation and the velocity structure near the source. The azimuth is obtained from the locations of the source and the recording station.

The incident angle at the source is obtained from the relation

$$P = \frac{r\sin(i)}{V}, \qquad (29)$$

where p is ray parameters from travel time

T(Δ) is the travel time at distance Δ given by

$$T(\Delta) = p\Delta + 2\int_{r_t}^{r_o} \frac{\sqrt{(r/v)^2 - p^2}}{r}$$ (Lay and Wallace, 1995)

r is radius of the earth

V is velocity at the source

r_t is the deepest point of penetration

Using the azimuth and angle of incidence at the source, the intersection of the rays to each station with the focal sphere are projected onto the equatorial plane of the focal sphere using the technique of lower hemisphere stereographic projection. The projections of the different points that indicate compressional and dilatational P arrivals define the orientations of the two nodal planes: auxiliary and fault planes. From the estimated configuration of fault plane and auxiliary plane, though difficult to identify uniquely from seismological data alone, the maximum (T) and minimum (P) tensional stress axes orientations can be obtained (Lay and Wallace 1995; Lowrie 1997). These two axes lie on a plane connecting the poles of the nodal planes in the compressional and dilatational quadrant, respectively, of the projection. Their orientation (trend and plunge) is determined by measuring 45^o along the connecting plane from either of the nodal planes.

By making use of the above basic assumptions fault plane solutions for five earthquakes were determined.

3.2.5. Estimation of b-values

b-value, a tectonic parameter describing the relative abundance of large to smaller shocks, is estimated using the magnitudes determined for the reported earthquakes. The computation of b-value is based on the Gutenberg and Richter (1956) magnitude – frequency relationship that defines the distribution of earthquakes with respect to magnitude. This relation is given by

$$\log N = a - bM_L, \qquad (30)$$

where N is the number of earthquakes having magnitudes M ≥ a given M_L, a and b are constants. A magnitude interval of 0.1ML is used. Completeness test of the catalogue was investigated first by considering the Gutenberg-Richter relationship at low magnitudes: departure from a straight line was interpreted as lack of completeness at low magnitudes. The M_L value at which the curve departs from a general straight line is taken as the threshold magnitude in the computation of the b-value.

Two methods were used in the estimation of b-values. The first one was a linear least-squares fit to the data. This technique was also used to test the reliability of the selected threshold magnitude by determining the residual of the fit (Figs. 12, 13 and14). The second

method was the maximum-likelihood method of Aki (1965). According to this method the b-value is expressed as

$$b = \frac{\log_{10}(e)}{M_{av} - M_{\min}} = \frac{0.43}{M_{av} - M_{\min}}, \qquad (31)$$

where M_{av} is the mean of the observed magnitudes and M_{min} is the minimum magnitude (threshold magnitude). According to Shi and Bolt (1982), the standard error (σ) of the maximum-likelihood estimation of b is approximated by

$$\sigma(b) = 2.30 * b^2 * \sigma(M_{av}), \qquad (32)$$

$$\sigma^2(M_{av}) = \frac{\sum_{i=1}^{n} (M_i - M_{av})^2}{n(n-1)}, \qquad (33)$$

where M_i's are the individual M_L values and n is the number of magnitude observations considered.

Separate b-values were estimated using the entire catalogue from this study and for the region where high seismic activity was observed. For this purpose earthquakes that lie outside the major study period were omitted. In addition, a b-value for the region where high seismicity was observed is also determined by including data from Keir (2006) for 2001.

4. RESULTS

4.1. Hypocenter Parameters

Hypocentral parameters of 144 earthquakes were finally obtained from the location programs (Appendix B). Earthquakes located within the network have higher accuracy with an average RMS (root-mean-square) of 0.5, while those falling outside the network have poor accuracy indicative of the effects of mainly bad station coverage. The Hypoinverse-2000 location output was then relocating using the double-difference algorithm of Waldhauser and Ellsworth (2002) and only 25 earthquakes fulfilled the defined location parameters. The similarity of the distribution of the 25 locations (Fig. 9a) from HypoDD (Fig. 9c) with the corresponding Hypoinverse-2000 (Fig. 9b) locations was taken as an evidence for the stability of the reported locations of the earthquakes in this study. The Hypoinverse-2000 locations are more diffuse than the corresponding HypoDD outputs. In both cases the epicenters form one cluster rather than showing any clear linear pattern with the fault structures in the region.

Seismic activity, during the study period, was distributed all along the rift system with relatively high concentration around 9^0N and 40^0E and 9.5^0N and 39.5^0E – near Dofen volcano and Ankober border fault (Fig. 10). Another prominent feature of the distribution is that the western rift margin has experienced relatively higher seismic activity than the eastern margin. Focal depth estimations, though determined without depth phases, range mainly from 7 to 14 km with average depth of 11 km.

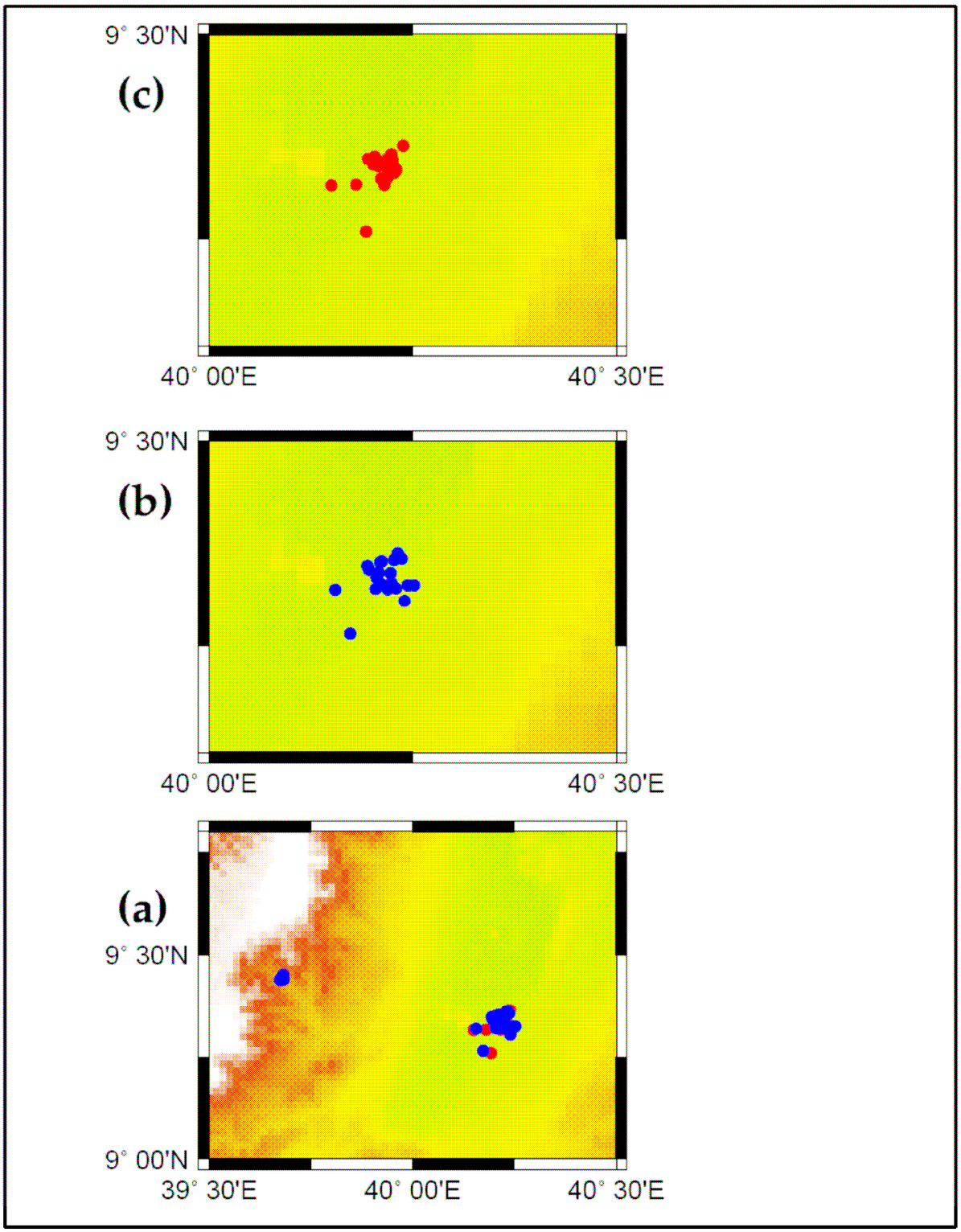

Figure 9. Comparison of the areal distribution of the 25 epicentral locations obtained from both programs (a) and separate plots of these locations (b) from Hypoinverse-2000 and (c) from HypoDD Red circles represent HypoDD locations and the blue ones represent Hypoinverse-2000 locations.

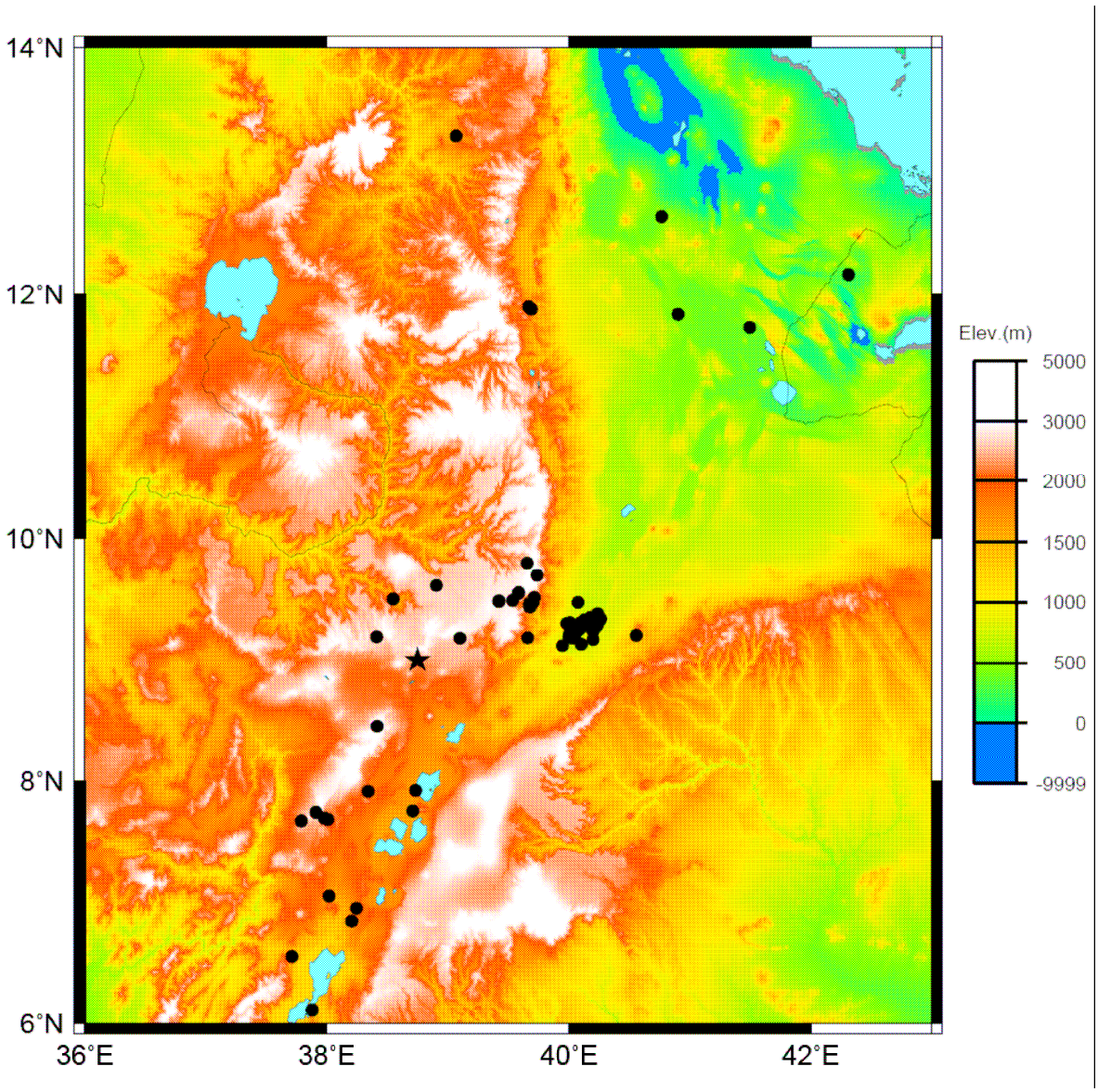

Figure 10. Distribution of epicenters determined for the period from May to July 2001, and some selected earthquakes in 2001. Black circles mark epicentral locations determined in this study. The black star is the location of Addis Ababa.

4.2. Fault Plane Solutions

The focal mechanisms estimated for four of the selected earthquakes that are located in the Ankober area show pure normal faulting on N-S trending faulting. The one located on the western escarpment also shows pure normal faulting but with a NW-SE trending fault plane (Table 2, Fig. 11). Geological observations (e.g. Wolfenden *et al*., 2005; Casey *et al*., 2006; Pizzi *et al*., 2006) revealed that the faults in Ankober area have high dips.

Table 2. Summary of source parameters determined from this study

No.	Date (YY/MM/DD)*	Or. Time (HH:MM:SS.SS)**	Lat. (^{O})	Lon. (^{O})	M_L	Strike	Dip	Rake
1	01/05/23	01:16:08.45	9.482	39.423	3.49	180/0	75/15	-90/-90
2	01/11/11	22:32:40.60	9.441	39.682	3.26	180/0	70/20	-90/-90
3	01/11/11	22:38:01.08	9.440	39.675	3.9	180/0	75/15	-90/-90
4	01/11/24	13:03:38.59	9.500	38.547	2.83	318/138	50/20	-90/-90
5	01/12/13	02:14:39.00	9.449	39.681	3.1	180/0	70/20	-90/-90

* YY/MM/DD – Year/Month/Day,

** HH:MM:SS.SS – Hour:Minute:Second

Table 3. P- and T-axis orientations of the focal mechanisms estimated

No.	Date (YY/MM/DD)	Or. Time (HH:MM:SS.SS)	T-axis		P-axis	
			Trend	Plunge	Trend	Plunge
1	01/05/23	01:16:08.45	270	30	90	60
2	01/11/11	22:32:40.60	270	25	90	65
3	01/11/11	22:38:01.08	270	30	90	60
4	01/11/24	13:03:38.59	48.16	5	228.16	85
5	01/12/13	02:14:39.00	270	25	90	65

The mechanisms do not show clear coincidence with exposed faults could be either due to buried origin or small offset by location error. Based on these observations, the nodal planes (Table 2) with high dip angle are considered to be fault planes. Although it is clear to determine extension directions for the respective mechanisms, numerical values of the P- and T-axis orientations are given in Table 3 measured from the assumed fault planes.

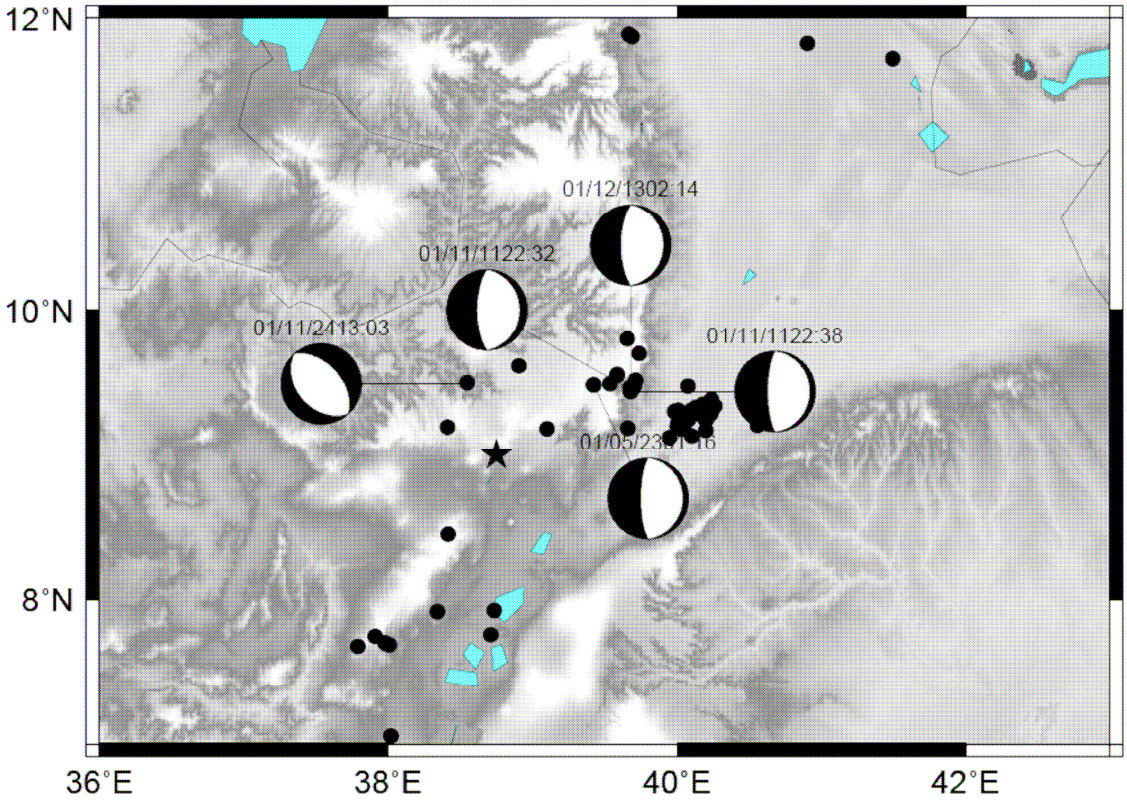

Figure 11. Plots of the five fault plane solutions determined in this study. Fault plane solutions are lower hemisphere projections. Black circles are epicentral locations from this study. Black star marks the location of Addis Ababa. The black parts of the 'beach-balls' represent the compressional quadrants of the focal sphere and the white parts represent the dilatational quadrants.

4.3. b-Values

First a b-value is determined using the catalogue for the period from May to July 2001. A least squares estimate of 1.22, using a threshold value of M_t = 2.9, was found (Fig. 12) and the maximum-likelihood estimate was 1.059±0.13.

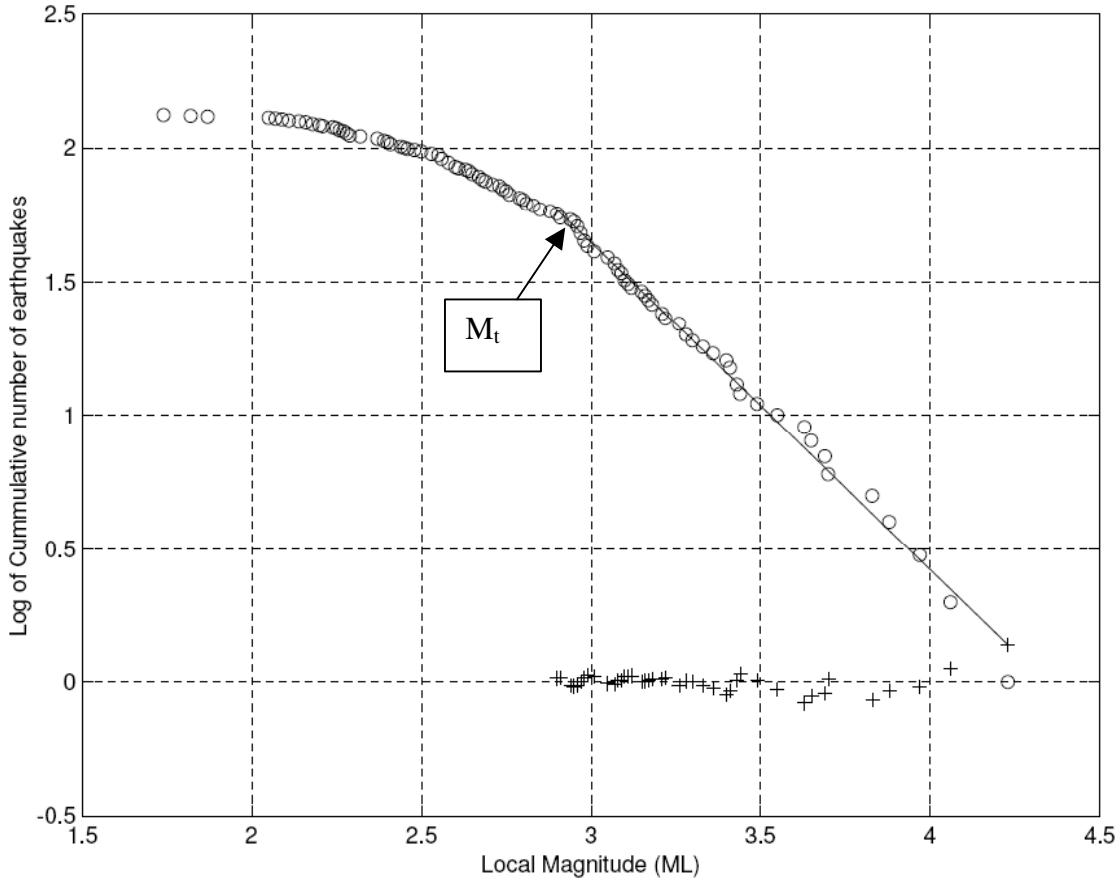

Figure 12. Frequency-Magnitude Distribution (FMD) plot of all earthquakes for the period between May and July, 2001. M_t is threshold magnitude ML=2.9 above which the catalogue is complete. The straight line is a least squares fit to the data above the threshold magnitude. The slope of the straight line is 1.22. The crosses are the residuals of the fit at each data point used in the least-squares estimation.

Separate b-value, using the same threshold magnitude, of 1.37 from the least squares method (Fig. 13) and a maximum-likelihood estimate of 1.17±0.16 was obtained for the area with high seismic activity (Fig. 10). The same data period as the above computation is used.

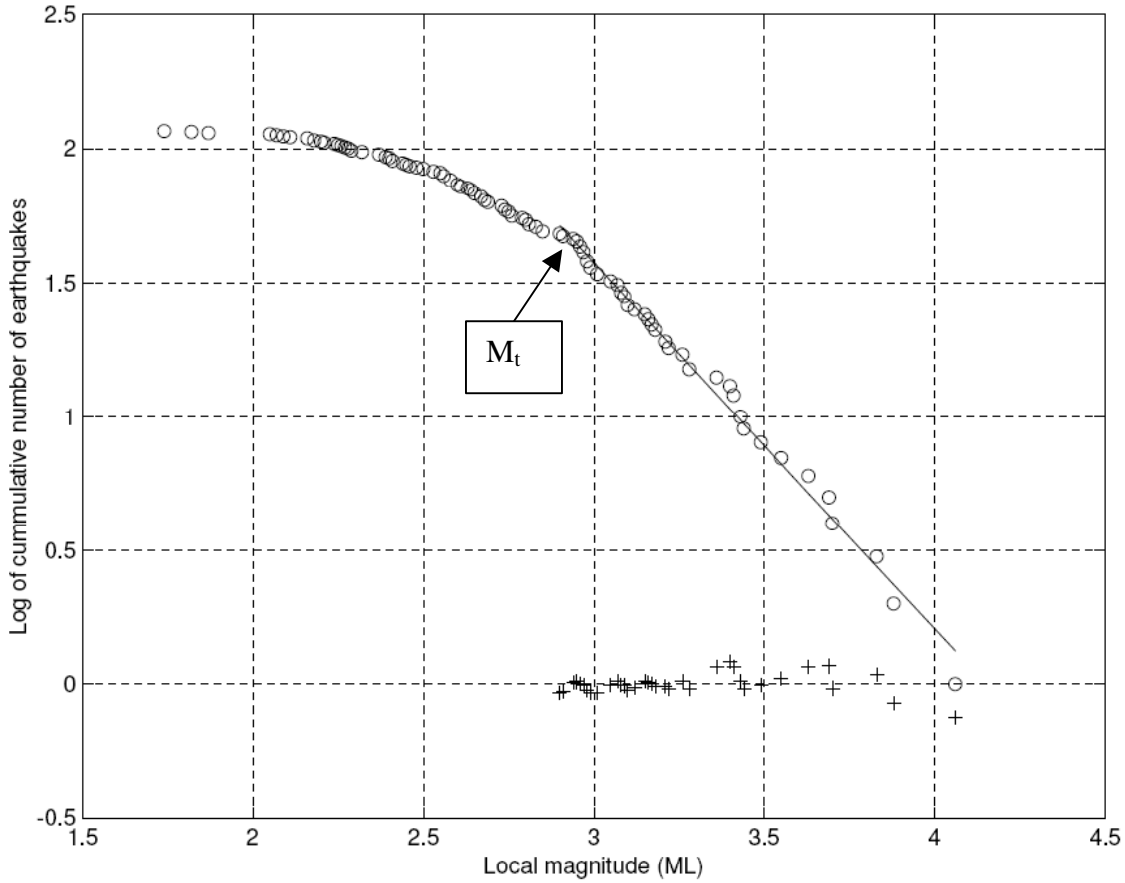

Figure 13. FMD plot of earthquakes located in the Ankober-Dofen area only for the time from May to July 2001. The least squares fit line has a slope of 1.37. Crosses are residuals of the fit at each data point. The threshold magnitude M_t is 2.9. The crosses are the residuals of the fit at each data point used in the least-squares estimation.

Finally, high b-value is estimated for the Ankober-Dofen area where high epicenter concentration is observed in this study. In this case, data obtained from the EAGLE network (Keir 2006) for the year 2001 was included. The data is complete above 2.1 M_L. The least-squares estimate is 0.91 (Fig. 14) and the maximum-likelihood method gave a b-value of 0.81±0.05.

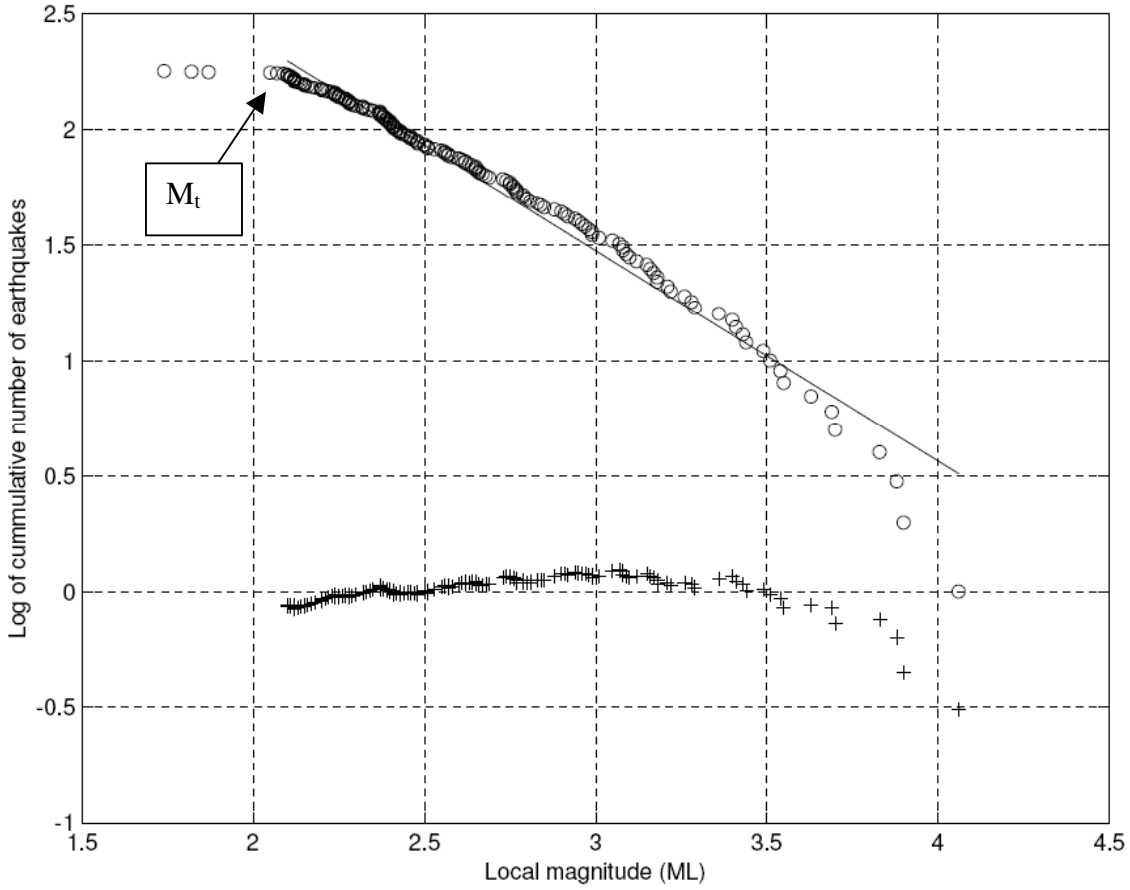

Figure 14. FMD plot of earthquakes located in the Ankober-Dofen area using data from this study and EAGLE for the year 2001. The threshold magnitude (M_t) is 2.1. The crosses are the residuals of the fit at each data point used in the least-squares estimate.

5. DISCUSSION

Although a small period is considered in this study, the distribution of epicenters observed agrees with the widely accepted idea of strain localization along the magmatic segments and continued seismic activity along the Ankober border fault. The highest seismicity from the Dofen Volcano area, which is part of the Dofen-Fentale magmatic segment, is a good manifestation of continued activity. The Quaternary, ~ 20 km-wide magmatic segments are zones of intensive dike injection (Keranen *et al.,* 2004; Bastow *et al*., 2005), and this diking activity is the major factor controlling seismicity, strain localization and faulting during continental breakup (Keir *et al.,* 2006a). The observed seismicity between May and July 2001, therefore, could be associated with some intrusion of magma or pure tectonic deformation.

Seismicity is also observed near the Ankober border fault where stress is believed to concentrate in this area due to the lateral density and lithospheric thickness contrast between the adjacent plateau and rift (e.g. Tiberi *et al*., 2005). The epicentral distribution in this area observed can be considered to show the fact that the Ankober Border fault is still experiencing strain (Wolfenden *et al.,* 2004) exceptionally from the other border faults as also revealed by Keir *et al.,* 2006a. The scattered epicenter distribution for the study period is also an indication of continued rifting process.

The normal faulting mechanisms determined in this study for all the events considered reveal extensional tectonic setting. The N-S trending normal fault plane solutions obtained for earthquakes from the Ankober area generally are similar with previous mechanisms of the

area (Keir *et al.,* 2006a), and could be associated with the N-S trending border faulting related to the Red Sea opening (Wolfenden *et al.,* 2004). E-W extension direction is obtained for four of the solutions. The exception is the focal mechanism determined for an earthquake located on the western plateau. It also shows pure normal faulting but trending NW-SE and with a NE-SW extension direction. It is similar with the Gewane activity (Ayele *et al.,* 2006) or Red Sea plate separation direction (Fig. 2). But it could possibly be a result of small-scale tectonics since structural observations show overall rift extension directions in the MER ranging from E-W to NW-SE (e.g. Boccaletti *et al.,* 1998; Bilham *et al.,* 1999; Wolfenden *et al.,* 2004; Acocela and Korme, 2002).

The relatively high b-values obtained both using the whole catalogue and data from the area with high seismicity show that seismic energy in the region is released mainly in the form of low magnitude earthquake. This similarity may not fully represent the b-value of the whole region as the large number of earthquakes from the Ankober-Dofen region influences the b-value determination in both cases. In terms of the stress condition near the focal region, the high b-values are manifestations that the region is characterized by low stress condition. The estimate obtained using a better data extent is lower in magnitude and has a better accuracy. This value shows a relatively higher stress condition in the Ankober -Dofen area. But the effects of both the data gap for some months in between and a wider time period should be taken into account. The maximum-likelihood estimates obtained from this study are close to the b-value of 1.13±0.05 determined by Keir *et al*., (2006b) for the MER.

6. CONCLUSIONS AND RECOMMENDATION

Earthquake data obtained mainly from the IRIS/PASSCAL Ethiopian seismic experiment for the months May to July 2001 were used to get insight into the recent rift activity. The major outcome of this work is the catalogue intended to partially fill (though small time period) the gap in time in the earthquake database of the country. A total of 144 hypocentral parameters are reported. Locations for earthquakes within the network were determined with high accuracy. The distribution shows the areas close to Ankober border fault and Dofen volcano had experienced relatively higher seismic activity during the study period. The majority of focal depths lie between 7 and 14 km. Local magnitude was also calculated for all the earthquakes reported in this study using the recent scale determined by Keir *et al.,* (2006b). To account for station corrections, an average of magnitude values determined by different stations is taken. Five of the source mechanisms show pure normal faulting. All but one trend N-S with E-W extension direction and could be associated with the N-S trending border faulting related to the Red Sea opening or simply local deformation. The exceptional one shows a mechanism that is pure normal faulting but trending NW-SE with NE-SW extension direction. Separate b-values were also determine using the catalogue of this study and by including data from EAGLE project. These estimates show that seismic energy was released in the region mainly in the form of small magnitude earthquakes. The proximity of the highly seismic area of this study to the Kesem Dam should be considered in the final stages of the construction.

To be able to get a clear picture and understand the processes associated with rift development and evolution, a wider time period should be considered. In addition, the use of

various seismological and/or other geophysical and geological approaches is recommended. Though it was impossible to fulfill these requirements at this stage, which was the major limitation of this study due to time constraint, a better result would be obtained if multidisciplinary approach were to be followed.

APPENDIX A - List of Amplitude readings for the 144 earthquakes measured on the horizontal components of two and more stations and the average magnitudes.

DATE – Date of the earthquake in Year/Month/Day

TIME – Origin time in Hour:Minute

STATION – Recording station code (Fig. 6)

DIST. – Epicentral distance of the recording station in kms

A_N (PTP) - Peak-to-Peak amplitude reading on the N-S component in millimeters

A_E (PTP) - Peak-to-Peak amplitude reading on the E-W component in millimeters

A_N/2 (ZTP) – Zero-to-peak amplitude on the N-S component

A_E/2 (ZTP) – Zero-To-Peak amplitude on the E-W component

ML-A_N – Local magnitude from the N-S component reading

ML-A_E – Local magnitude from the E-W component reading

ML(av) – Average local magnitude from the N-S and E-W components

ML – final Local Magnitude value for the earthquake

DATE	TIME	STATION	DIST. (km)	A_N(PTP)	A_E(PTP)	A_N/2(ZTP)	A_E/2(ZTP)	ML-A_N	ML-A_E	ML(av)	ML
01/05/10	16:51	FURI	44.2	2.6564	1.8480	1.3282	0.9240	2.6490	2.4914	2.57	2.83
		DMRK	144.3	1.2209	1.6526	0.6104	0.8263	3.0331	3.1646	3.10	
01/05/11	17:30	ARBA	89.6	2.9037	3.6057	1.4518	1.8028	3.1034	3.1974	3.15	3.3
		TERC	213.8	1.3007	2.1261	0.6503	1.0631	3.3391	3.5525	3.45	
01/05/12	01:44	FURI	123.5	3.3450	3.3450	1.6725	1.6725	3.3678	3.3678	3.37	3.18
		BUTA	207	0.8887	0.7342	0.4444	0.3671	3.1496	3.0667	3.11	
		HOSA	291.2	0.3278	0.4741	0.1639	0.2371	2.9837	3.1439	3.06	
01/05/12	02:07	FURI	122.6	4.1127	2.8574	2.0564	1.4287	3.4527	3.2946	3.37	3.26
		BUTA	206.1	1.1995	1.0346	0.5997	0.5173	3.2766	3.2124	3.24	
		HOSA	290.2	0.4328	0.5966	0.2164	0.2983	3.1015	3.2409	3.17	
01/05/14	23:11	FURI	114.6	0.6689	0.8872	0.3344	0.4436	2.6204	2.7430	2.68	2.91
		DMRK	217.7	0.7028	0.8965	0.3514	0.4482	3.0853	3.1910	3.14	
01/05/18	13:49	FURI	129.3	1.9959	1.2768	0.9980	0.6384	3.1736	2.9795	3.08	2.58
		WASH	74.2	1.0230	1.5552	0.5115	0.7776	2.5358	2.7177	2.63	
		FICH	111.1	0.1499	0.2152	0.0750	0.1076	1.9510	2.1080	2.03	
01/05/18	18:08	ARBA	116.4	17.1216	21.1609	8.5608	10.5805	4.0386	4.1306	4.08	4.23
		FURI	416.7	2.5057	3.3560	1.2529	1.6780	4.1871	4.3139	4.25	
		BAHI	646.3	1.3167	1.1720	0.6583	0.5860	4.3805	4.3300	4.36	
01/05/18	20:33	HOSA	21.3	7.3709	7.2823	3.6855	3.6411	2.6883	2.6830	2.69	2.27
		BUTA	63.1	0.6586	0.7063	0.3293	0.3531	2.2485	2.2789	2.26	

		SELA	128.3	0.1278	0.1098	0.0639	0.0549	1.9748	1.9087	1.94	
		ARBA	185.9	0.1119	0.1206	0.0559	0.0603	2.1712	2.2039	2.19	
01/05/19	03:28	WASH	24.9	5.6030	4.1889	2.8015	2.0944	2.6542	2.5279	2.59	2.58
		FURI	153.7	0.5200	0.4555	0.2600	0.2278	2.7053	2.6478	2.68	
		FICH	158.5	0.3264	0.2490	0.1632	0.1245	2.5242	2.4066	2.47	
01/05/19	11:18	WASH	27	17.6672	10.8410	8.8336	5.4205	3.1973	2.9852	3.09	2.95
		WANE	127.2	0.5176	1.6120	0.2588	0.8060	2.5767	3.0700	2.82	
		FURI	152.4	1.3517	0.8877	0.6758	0.4439	3.1144	2.9318	3.02	
		FICH	156.4	0.8461	0.6213	0.4230	0.3106	2.9286	2.7945	2.86	
01/05/19	18:49	TEND	148	4.1740	5.0961	2.0870	2.5480	3.5841	3.6708	3.63	3.97
		WANE	285.3	5.9369	7.4111	2.9684	3.7055	4.2247	4.3210	4.27	
		WASH	421.9	3.2225	3.2635	1.6113	1.6317	4.3083	4.3138	4.31	
		FICH	471.1	0.4894	0.4280	0.2447	0.2140	3.5996	3.5413	3.57	
		ARBA	853.5	0.2573	0.3235	0.1286	0.1618	4.0369	4.1364	4.09	
01/05/20	09:58	WASH	27.3	10.5878	8.7138	5.2939	4.3569	2.9810	2.8964	2.94	2.81
		FURI	150.2	0.9310	0.6208	0.4655	0.3104	2.9425	2.7666	2.85	
		FICH	155	0.5417	0.3788	0.2708	0.1894	2.7288	2.5734	2.65	
01/05/21	19:23	WASH	33.1	3.6633	2.5932	1.8317	1.2966	2.6264	2.4764	2.55	2.37
		FURI	151.5	0.3389	0.2280	0.1694	0.1140	2.5095	2.3373	2.42	
		FICH	152	0.1523	0.1395	0.0762	0.0697	2.1644	2.1263	2.15	
01/05/21	20:09	WASH	74.2	0.4966	0.7324	0.2483	0.3662	2.2220	2.3907	2.31	2.16
		FICH	111.2	0.1964	0.1585	0.0982	0.0793	2.0688	1.9759	2.02	
01/05/21	21:12	HOSA	20.2	3.2146	4.3379	1.6073	2.1690	2.2992	2.4293	2.36	2.25
		TERC	108	0.2558	0.2328	0.1279	0.1164	2.1650	2.1241	2.14	
01/05/22	03:49	WASH	44	1.1173	1.9636	0.5587	0.9818	2.2703	2.5152	2.39	2.39
		FURI	179.5	0.2520	0.2396	0.1260	0.1198	2.4989	2.4769	2.49	
		FICH	170.6	0.1371	0.1998	0.0685	0.0999	2.1986	2.3622	2.28	
01/05/22	16:10	WASH	30.2	10.2731	6.0995	5.1366	3.0497	3.0235	2.7971	2.91	2.67
		WANE	126.7	0.2901	0.5274	0.1450	0.2637	2.3226	2.5822	2.45	
		FURI	150.5	0.6889	0.6621	0.3444	0.3310	2.8131	2.7958	2.80	
		FICH	153.3	0.3547	0.3428	0.1773	0.1714	2.5373	2.5225	2.53	
01/05/23	01:16	FICH	82.3	10.4334	5.4609	5.2167	2.7304	3.6069	3.3257	3.47	3.49
		FURI	104.2	22.9589	15.2395	11.4795	7.6198	4.0954	3.9174	4.01	
		WASH	98.1	9.5994	8.7307	4.7997	4.3653	3.6788	3.6376	3.66	
		DIYA	260.9	2.6443	2.7155	1.3222	1.3577	3.8010	3.8125	3.81	
		SELA	169.9	1.0086	0.9449	0.5043	0.4725	3.0624	3.0340	3.05	
		ARBA	430.1	0.1410	0.1233	0.0705	0.0617	2.9682	2.9099	2.94	
01/01/24	08:10	BIRH	27	3.2683	2.7024	1.6342	1.3512	2.4645	2.3819	2.42	2.75
		WASH	76.5	1.6198	2.7861	0.8099	1.3930	2.7538	2.9893	2.87	
		BAHI	341.2	0.2909	0.1718	0.1454	0.0859	3.0674	2.8386	2.95	
01/05/24	19:55	WASH	30.6	2.5019	1.6305	1.2509	0.8153	2.4173	2.2314	2.32	2.2
		FURI	152.3	0.1418	0.1462	0.0709	0.0731	2.1346	2.1480	2.14	
		FICH	154.1	0.2061	0.0966	0.1031	0.0483	2.3052	1.9762	2.14	
01/05/24	20:24	BIRH	23.6	0.6905	0.7816	0.3453	0.3908	1.7157	1.7695	1.74	1.74
		FICH	82	0.2061	0.0966	0.1031	0.0483	1.9004	1.5714	1.74	
01/05/24	21:14	WASH	28.5	2.2231	1.9129	1.1115	0.9564	2.3268	2.2615	2.29	2.11
		FURI	148.2	0.1613	0.1243	0.0806	0.0622	2.1721	2.0590	2.12	
		FICH	153.2	0.0986	0.0700	0.0493	0.0350	1.9810	1.8321	1.91	
01/05/24	21:19	WASH	28.1	2.2230	1.3495	1.1115	0.6748	2.3190	2.1022	2.21	2.26

		FURI	148.6	0.1601	0.1134	0.0801	0.0567	2.1708	2.0210	2.10	
		FICH	153.7	0.3787	0.2624	0.1893	0.1312	2.5675	2.4082	2.49	
01/05/24	21:26	WASH	17.2	9.1885	6.9589	4.5943	3.4795	2.6685	2.5478	2.61	2.6
		FURI	158.6	0.6908	0.4581	0.3454	0.2290	2.8502	2.6718	2.76	
		WANE	129.4	0.2131	0.7290	0.1066	0.3645	2.2025	2.7367	2.47	
		FICH	166.3	0.3787	0.2624	0.1893	0.1312	2.6219	2.4626	2.54	
01/05/25	18:28	WASH	30.4	4.7029	2.6637	2.3515	1.3319	2.6878	2.4409	2.56	2.44
		FURI	150.1	0.3074	0.2691	0.1537	0.1345	2.4609	2.4030	2.43	
		FICH	152.9	0.1733	0.2645	0.0867	0.1322	2.2246	2.4081	2.32	
01/05/25	21:05	WASH	28.2	2.6539	1.7983	1.3269	0.8992	2.3979	2.2289	2.31	2.32
		FICH	151.6	0.1292	0.0826	0.0646	0.0413	2.0911	1.8969	1.99	
		DMRK	276.5	0.1496	0.1933	0.0748	0.0966	2.6004	2.7116	2.66	
01/05/25	22:19	DIYA	169.9	0.8611	1.1236	0.4305	0.5618	2.9937	3.1093	3.05	3.65
		WANE	384.8	1.1695	0.8758	0.5848	0.4379	3.7807	3.6551	3.72	
		FICH	388.6	0.5501	0.6636	0.2751	0.3318	3.4623	3.5438	3.50	
		HOSA	646	1.0408	1.2124	0.5204	0.6062	4.2778	4.3441	4.31	
01/05/26	20:10	TEND	53.9	8.7959	9.7251	4.3980	4.8625	3.2824	3.3261	3.30	3.33
		KARA	223.3	0.9300	1.1336	0.4650	0.5668	3.2262	3.3121	3.27	
		DMRK	440.6	0.3183	0.4291	0.1591	0.2145	3.3454	3.4751	3.41	
01/05/28	06:42	WASH	29.1	27.6409	19.8999	13.8205	9.9499	3.4329	3.2902	3.36	3.41
		FURI	152.9	2.0528	1.7226	1.0264	0.8613	3.2981	3.2219	3.26	
		DMRK	280.1	1.3889	1.5789	0.6945	0.7895	3.5787	3.6344	3.61	
01/05/30	20:19	WASH	31	11.3004	9.2650	5.6502	4.6325	3.0793	2.9931	3.04	3.07
		FURI	152.9	0.8875	0.9421	0.4438	0.4711	2.9339	2.9598	2.95	
		DMRK	278.9	0.6322	0.6109	0.3161	0.3054	3.2334	3.2184	3.23	
01/05/30	22:38	WASH	31.5	1.8689	1.4548	0.9345	0.7274	2.3066	2.1979	2.25	2.18
		KARA	131.5	0.2142	0.2651	0.1071	0.1325	2.2154	2.3079	2.26	
		FICH	153.5	0.0963	0.1176	0.0481	0.0588	1.9719	2.0589	2.02	
01/06/02	23:10	CHEF	69.9	1.9713	3.1355	0.9856	1.5678	2.7851	2.9867	2.89	2.71
		TERC	88.6	1.2656	0.9570	0.6328	0.4785	2.7358	2.6144	2.68	
		HOSA	113.4	0.6365	0.5447	0.3183	0.2723	2.5921	2.5244	2.56	
01/06/04	11:38	WASH	36.5	1.2866	1.4966	0.6433	0.7483	2.2264	2.2921	2.26	2.55
		FURI	171.5	0.5257	0.4876	0.2629	0.2438	2.7860	2.7533	2.77	
		FICH	166.5	0.3370	0.4276	0.1685	0.2138	2.5722	2.6756	2.62	
01/06/04	22:56	WASH	38.9	5.3752	6.9484	2.6876	3.4742	2.8830	2.9945	2.94	3.09
		FICH	168.8	1.0607	1.4430	0.5304	0.7215	3.0797	3.2134	3.15	
		FURI	175	1.5084	1.0853	0.7542	0.5427	3.2580	3.1150	3.19	
01/06/04	23:12	WASH	39.7	3.8802	6.9484	1.9401	3.4742	2.7529	3.0060	2.88	3.01
		FURI	173.9	1.3040	1.1252	0.6520	0.5626	3.1903	3.1263	3.16	
		FICH	167.1	0.7597	1.0671	0.3798	0.5336	2.9277	3.0752	3.00	
01/06/05	01:58	WASH	39.9	2.7198	4.1140	1.3599	2.0570	2.6014	2.7812	2.69	2.69
		FURI	172.5	0.4156	0.4952	0.2078	0.2476	2.6879	2.7641	2.73	
		FICH	165.6	0.3559	0.4775	0.1779	0.2387	2.5920	2.7197	2.66	
01/06/08	01:25	TEND	11.7	38.6893	39.3408	19.3447	19.6704	3.0867	3.0939	3.09	3.05
		DMRK	385.8	0.1916	0.2028	0.0958	0.1014	2.9975	3.0223	3.01	
01/06/08	07:47	TEND	95.6	1.5016	1.4908	0.7508	0.7454	2.8571	2.8539	2.86	2.96
		FICH	385.1	0.2110	0.2457	0.1055	0.1228	3.0377	3.1038	3.07	
01/06/09	05:00	DIYA	10.1	99.6819	82.3741	49.8410	41.1871	3.4196	3.3367	3.38	3.11

		KARA	165.3	1.5006	2.1589	0.7503	1.0794	3.2158	3.3737	3.29	
		BIRH	246.1	0.2805	0.2589	0.1403	0.1295	2.7804	2.7457	2.76	
		FICH	254.7	0.3935	0.4665	0.1968	0.2333	2.9545	3.0284	2.99	
01/06/10	02:53	DIYA	11.4	23.8594	26.0900	11.9297	13.0450	2.8629	2.9017	2.88	2.88
		BAHI	252.8	0.1184	0.1688	0.0592	0.0844	2.4269	2.5810	2.50	
		DMRK	275.8	0.5801	0.7745	0.2901	0.3873	3.1869	3.3124	3.25	
01/06/14	00:48	BELA	100.5	1.3506	1.2519	0.6753	0.6259	2.8423	2.8093	2.83	2.9
		HOSA	88.1	2.7454	2.7794	1.3727	1.3897	3.0687	3.0740	3.07	
		TERC	118.5	0.8054	1.0891	0.4027	0.5446	2.7226	2.8536	2.79	
01/06/14	05:16	BIRH	23.6	3.5927	6.3150	1.7964	3.1575	2.4320	2.6769	2.55	2.61
		FICH	110.3	0.5378	0.4339	0.2689	0.2170	2.5012	2.4080	2.45	
		WANE	112.5	0.9990	1.1927	0.4995	0.5963	2.7827	2.8597	2.82	
01/06/14	23:32	BUTA	44.3	1.4647	2.0928	0.7324	1.0464	2.3917	2.5467	2.47	2.14
		BIRH	214	0.0339	0.0438	0.0169	0.0219	1.7554	1.8669	1.81	
01/06/15	00:19	BUTA	37.6	1.9705	2.9548	0.9852	1.4774	2.4281	2.6041	2.52	2.56
		TERC	199.4	0.2428	0.1671	0.1214	0.0836	2.5587	2.3963	2.48	
		DMRK	218.4	0.2369	0.3396	0.1184	0.1698	2.6154	2.7719	2.69	
01/06/17	23:23	WASH	37.9	0.8265	1.9425	0.4132	0.9712	2.0553	2.4264	2.24	2.21
		FICH	168.9	0.1237	0.1381	0.0619	0.0691	2.1469	2.1948	2.17	
01/06/17	23:24	WASH	37.8	1.3356	3.2008	0.6678	1.6004	2.2622	2.6418	2.45	2.5
		FICH	169.3	0.2737	0.3424	0.1369	0.1712	2.4935	2.5908	2.54	
01/06/17	23:55	WASH	37.6	1.3063	3.5351	0.6532	1.7676	2.2496	2.6820	2.47	2.56
		FICH	169.5	0.3650	0.4351	0.1825	0.2175	2.6193	2.6956	2.66	
01/06/18	00:18	WASH	38.1	2.0948	4.8448	1.0474	2.4224	2.4621	2.8263	2.64	2.64
		FICH	168.7	0.3685	0.4130	0.1842	0.2065	2.6201	2.6696	2.64	
01/06/19	22:56	WASH	36.2	3.6048	4.0356	1.8024	2.0178	2.6692	2.7183	2.69	2.83
		FICH	166.3	0.3181	0.3524	0.1591	0.1762	2.5463	2.5907	2.57	
		DMRK	290.2	0.5642	0.5801	0.2821	0.2901	3.2167	3.2287	3.22	
01/06/20	12:34	BIRH	20.3	1.0599	0.8998	0.5300	0.4499	1.8200	1.7489	1.78	1.82
		FICH	101	0.1546	0.1294	0.0773	0.0647	1.9042	1.8268	1.87	
01/06/22	11:27	WASH	34.8	2.6685	3.4284	1.3342	1.7142	2.5166	2.6255	2.57	2.56
		BIRH	84.8	0.3645	0.4952	0.1822	0.2476	2.1684	2.3014	2.23	
		FICH	169.3	0.6376	0.7106	0.3188	0.3553	2.8607	2.9078	2.88	
01/06/22	14:09	WASH	28.8	5.4206	6.7631	2.7103	3.3816	2.7196	2.8157	2.77	2.73
		BIRH	74.5	0.4909	0.8851	0.2455	0.4425	2.2194	2.4754	2.35	
		FICH	153.5	1.0240	1.3955	0.5120	0.6978	2.9987	3.1331	3.07	
01/06/22	14:18	WASH	30.4	1.8932	3.5778	0.9466	1.7889	2.2926	2.5690	2.43	2.55
		FICH	158.5	0.4092	0.5102	0.2046	0.2551	2.6224	2.7181	2.67	
01/06/22	14:52	BIRH	81.2	0.5791	1.5160	0.2896	0.7580	2.3431	2.7610	2.55	2.95
		FICH	166.4	1.4358	1.6596	0.7179	0.8298	3.2012	3.2641	3.23	
		BAHI	393	0.2394	0.1963	0.1197	0.0982	3.1115	3.0254	3.07	
01/06/22	23:40	WASH	37.4	29.4668	43.0428	14.7334	21.5214	3.5999	3.7645	3.68	3.63
		FICH	169.6	4.9974	3.6533	2.4987	1.8267	3.7562	3.6201	3.69	
		BAHI	396.5	0.6831	0.5196	0.3415	0.2598	3.5752	3.4564	3.52	
01/06/23	05:42	WASH	30.8	0.9931	1.3448	0.4965	0.6724	2.0196	2.1513	2.09	2.27
		FICH	156.4	0.2656	0.3017	0.1328	0.1509	2.4255	2.4809	2.45	
01/06/23	13:20	WASH	36.9	13.5736	14.1011	6.7868	7.0505	3.2558	3.2723	3.26	3.44
		BIRH	85.6	1.5260	2.1656	0.7630	1.0828	2.7960	2.9480	2.87	
		FICH	170.6	3.0928	3.3376	1.5464	1.6688	3.5519	3.5850	3.57	

		DMRK	294.3	3.3852	4.3279	1.6926	2.1640	4.0064	4.1131	4.06	
01/06/23	19:09	WASH	39.1	28.6440	47.1405	14.3220	23.5702	3.6125	3.8289	3.72	3.7
		BAHI	396.5	0.7768	0.9271	0.3884	0.4636	3.6311	3.7079	3.67	
01/06/23	19:12	WASH	37.8	54.7644	46.7089	27.3822	23.3544	3.8751	3.8060	3.84	3.83
		BIRH	85.7	4.3295	6.6812	2.1647	3.3406	3.2496	3.4380	3.34	
		NAZA	132.5	10.0293	18.5344	5.0147	9.2672	3.8908	4.1575	4.02	
		FICH	170.8	9.9928	12.2951	4.9964	6.1476	4.0620	4.1521	4.11	
01/06/23	19:16	WASH	35.7	4.9543	4.3962	2.4772	2.1981	2.7996	2.7477	2.77	2.96
		KARA	127.2	7.0381	0.7294	3.5191	0.3647	3.7101	2.7256	3.22	
		FICH	171.5	0.6528	0.6831	0.3264	0.3415	2.8800	2.8997	2.89	
01/06/23	19:29	WASH	34.5	1.5830	2.8129	0.7915	1.4064	2.2850	2.5347	2.41	2.41
01/06/23	20:00	WASH	37.2	49.3975	84.9766	24.6988	42.4883	3.8213	4.0569	3.94	4.06
		NAZA	132.6	14.6448	25.5234	7.3224	12.7617	4.0557	4.2970	4.18	
		FICH	171.6	6.9934	6.7681	3.4967	3.3841	3.9103	3.8961	3.90	
		HOSA	325.6	4.5797	4.2102	2.2898	2.1051	4.2236	4.1871	4.21	
01/06/24	01:47	KARA	122.6	1.4010	1.1828	0.7005	0.5914	2.9851	2.9115	2.95	3.07
		TERC	412.4	0.2926	0.2216	0.1463	0.1108	3.2445	3.1237	3.18	
01/06/24	02:19	WASH	36.4	4.5640	9.7231	2.2820	4.8616	2.7748	3.1032	2.94	3.08
		FICH	163.9	1.3457	1.7223	0.6729	0.8612	3.1625	3.2697	3.22	
01/06/24	03:53	WASH	37.1	9.6057	11.8152	4.8028	5.9076	3.1086	3.1985	3.15	3.15
		FICH	169.1	1.0097	1.5188	0.5048	0.7594	3.0595	3.2368	3.15	
01/06/24	05:24	WASH	46	2.0135	3.9240	1.0068	1.9620	2.5513	2.8411	2.70	2.79
		FICH	217.5	0.4544	0.4328	0.2272	0.2164	2.8953	2.8741	2.88	
01/06/24	07:26	WASH	40.6	3.4687	7.8006	1.7344	3.9003	2.7169	3.0688	2.89	2.98
		FICH	172	0.9679	1.0785	0.4840	0.5392	3.0531	3.1001	3.08	
01/06/24	10:42	WASH	33.6	0.3099	0.3956	0.1549	0.1978	1.5620	1.6681	1.62	2.09
		BIRH	83.5	0.3378	0.2470	0.1689	0.1235	2.1259	1.9900	2.06	
		FICH	167.7	0.3098	0.3957	0.1549	0.1978	2.5406	2.6469	2.59	
01/06/24	10:46	WASH	39.3	11.5486	9.7589	5.7743	4.8795	3.2209	3.1478	3.18	3.16
		FICH	173.9	1.0975	1.1569	0.5488	0.5785	3.1154	3.1383	3.13	
01/06/24	10:55	WASH	34.2	1.2043	2.7910	0.6022	1.3955	2.1614	2.5264	2.34	2.45
		FICH	160.2	0.3881	0.3032	0.1940	0.1516	2.6067	2.4995	2.55	
01/06/24	13:21	WASH	30.2	5.3345	9.9749	2.6673	4.9875	2.7389	3.0107	2.87	2.99
		FICH	155.5	1.2705	1.2366	0.6353	0.6183	3.1012	3.0895	3.10	
01/06/24	18:17	WASH	36.5	3.0522	4.2055	1.5261	2.1027	2.6016	2.7408	2.67	2.8
		FICH	170.9	0.6992	0.7783	0.3496	0.3892	2.9073	2.9539	2.93	
01/06/24	18:23	WASH	38.9	4.0581	5.4337	2.0291	2.7169	2.7610	2.8877	2.82	2.97
		FICH	170.5	1.1415	1.0984	0.5707	0.5492	3.1186	3.1019	3.11	
01/06/24	19:26	WASH	32.9	0.7616	0.9047	0.3808	0.4524	1.9409	2.0157	1.98	2.07
		FICH	163.3	0.1060	0.1683	0.0530	0.0842	2.0564	2.2571	2.16	
01/06/24	20:25	WASH	37.8	1.0661	1.1785	0.5330	0.5893	2.1643	2.2079	2.19	2.25
		FICH	173.4	0.1649	0.1765	0.0824	0.0883	2.2902	2.3198	2.31	
01/06/25	00:41	WASH	30.9	1.0593	1.5004	0.5297	0.7502	2.0495	2.2006	2.13	2.28
		BIRH	88.1	0.2892	0.3008	0.1446	0.1504	2.0913	2.1083	2.10	
		FICH	172	0.3707	0.3465	0.1853	0.1732	2.6363	2.6070	2.62	
01/06/25	00:47	WASH	40.5	5.2849	10.0623	2.6425	5.0311	2.8983	3.1780	3.04	2.99
		BIRH	83.3	1.1462	1.2730	0.5731	0.6365	2.6551	2.7006	2.68	
		FICH	168.8	1.7210	1.5140	0.8605	0.7570	3.2899	3.2342	3.26	
01/06/25	06:58	WASH	35.8	5.6075	10.4375	2.8037	5.2188	2.8549	3.1248	2.99	3.21

		BIRH	88.4	2.1375	2.9574	1.0687	1.4787	2.9620	3.1030	3.03	
		FICH	173.3	3.2781	3.5810	1.6391	1.7905	3.5882	3.6266	3.61	
01/06/25	07:09	WASH	38.9	2.0443	3.8309	1.0221	1.9155	2.4632	2.7359	2.60	2.63
		BIRH	85.9	0.5460	0.5722	0.2730	0.2861	2.3518	2.3721	2.36	
		FICH	171.2	0.7932	0.7130	0.3966	0.3565	2.9634	2.9171	2.94	
01/06/25	07:16	WASH	35.4	2.8687	3.6119	1.4344	1.8060	2.5576	2.6576	2.61	2.76
		FICH	164.7	0.7030	0.8002	0.3515	0.4001	2.8839	2.9401	2.91	
01/06/25	07:37	WASH	39	3.2768	5.8271	1.6384	2.9136	2.6695	2.9195	2.79	2.96
		FICH	169.6	1.0694	1.2957	0.5347	0.6478	3.0866	3.1699	3.13	
01/06/25	08:14	WASH	38	1.7551	3.3693	0.8775	1.6846	2.3838	2.6670	2.53	2.65
		FICH	164.6	0.5835	0.5053	0.2917	0.2527	2.8026	2.7401	2.77	
01/06/25	08:26	WASH	38.8	4.6612	9.0879	2.3306	4.5439	2.8197	3.1097	2.96	3.17
		FICH	170	2.0951	2.1000	1.0475	1.0500	3.3803	3.3813	3.38	
01/06/25	09:14	WASH	38.2	18.0284	25.3909	9.0142	12.6954	3.3984	3.5471	3.47	3.55
		BAHI	400	0.8191	0.6922	0.4096	0.3461	3.6624	3.5893	3.63	
01/06/25	09:46	WASH	33.7	7.0910	10.5963	3.5455	5.2981	2.9232	3.0977	3.01	3.09
		FICH	162.2	1.2662	1.5533	0.6331	0.7767	3.1288	3.2176	3.17	
01/06/25	10:20	WASH	33.4	1.7379	2.7955	0.8689	1.3977	2.3075	2.5140	2.41	2.5
		BIRH	76	0.5925	0.5889	0.2963	0.2945	2.3131	2.3104	2.31	
		FICH	159.1	0.5972	0.5450	0.2986	0.2725	2.7891	2.7494	2.77	
01/06/25	11:08	WASH	33.7	2.5015	3.4862	1.2508	1.7431	2.4707	2.6148	2.54	2.73
		FICH	161.7	0.8121	0.7768	0.4060	0.3884	2.9338	2.9145	2.92	
01/06/25	16:38	WASH	39.7	2.8489	4.2502	1.4244	2.1251	2.6187	2.7925	2.71	2.94
		FICH	173.4	1.2013	1.3342	0.6007	0.6671	3.1526	3.1982	3.18	
01/06/25	16:39	WASH	38.5	3.8994	5.0337	1.9497	2.5169	2.7378	2.8487	2.79	2.97
		FICH	170.1	1.1706	1.3160	0.5853	0.6580	3.1279	3.1787	3.15	
01/06/25	16:53	WASH	38.9	1.1353	1.8834	0.5677	0.9417	2.2077	2.4276	2.32	2.41
		FICH	166.9	0.2675	0.3158	0.1337	0.1579	2.4734	2.5456	2.51	
01/06/25	16:56	WASH	39.4	0.7781	1.2341	0.3890	0.6171	2.0508	2.2512	2.15	2.32
		FICH	169.6	0.2744	0.2546	0.1372	0.1273	2.4957	2.4634	2.48	
01/06/25	16:59	WASH	39.9	2.7372	4.1298	1.3686	2.0649	2.6042	2.7828	2.69	2.8
		BIRH	86.5	0.6712	1.0098	0.3356	0.5049	2.4457	2.6230	2.53	
		FICH	172	1.4682	1.1453	0.7341	0.5726	3.2341	3.1262	3.18	
01/06/25	17:03	WASH	38	11.3042	22.7073	5.6521	11.3536	3.1927	3.4957	3.34	3.43
		FICH	173	2.6474	2.8220	1.3237	1.4110	3.4942	3.5219	3.51	
01/06/25	17:36	WASH	40.1	2.1331	2.5329	1.0665	1.2664	2.4987	2.5733	2.54	2.68
		FICH	174.4	0.5682	0.5382	0.2841	0.2691	2.8315	2.8080	2.82	
01/06/26	12:46	WASH	36.6	4.1831	5.5422	2.0915	2.7711	2.7400	2.8622	2.80	2.97
		FICH	165.3	1.0543	1.4455	0.5272	0.7228	3.0625	3.1995	3.13	
01/06/26	17:33	WASH	38.7	4.5959	7.9067	2.2980	3.9534	2.8121	3.0477	2.93	3.05
		FICH	165.8	1.6211	1.1325	0.8105	0.5662	3.2514	3.0956	3.17	
01/06/26	17:39	WASH	39.5	6.0221	14.4214	3.0110	7.2107	2.9410	3.3202	3.13	3.28
		BIRH	84	1.9383	3.4967	0.9691	1.7483	2.8883	3.1446	3.02	
		FICH	169.3	3.5139	3.3443	1.7569	1.6722	3.6020	3.5805	3.59	
		BAHI	395.5	0.4467	0.4113	0.2233	0.2057	3.3884	3.3526	3.37	
01/06/26	22:15	WASH	37.6	0.9877	1.3986	0.4938	0.6993	2.1282	2.2793	2.20	2.28
		FICH	165.8	0.2222	0.1986	0.1111	0.0993	2.3883	2.3395	2.36	
01/06/26	22:22	WASH	41.9	35.1152	77.8301	17.5576	38.9151	3.7400	4.0856	3.91	3.69
		BIRH	84.9	2.7646	7.8411	1.3823	3.9206	3.0490	3.5018	3.28	

		FICH	170.6	9.0269	9.6926	4.5135	4.8463	4.0171	4.0480	4.03	
		BAHI	395.7	0.9611	0.8233	0.4806	0.4116	3.7216	3.6544	3.69	
		TERC	416.9	0.5599	0.5522	0.2799	0.2761	3.5367	3.5307	3.53	
01/06/26	22:32	WASH	41	75.6320	142.9731	37.8160	71.4866	4.0609	4.3375	4.20	3.88
		BIRH	84.7	5.9960	8.1606	2.9980	4.0803	3.3838	3.5177	3.45	
		FICH	170.3	10.8458	15.3304	5.4229	7.6652	4.0956	4.2459	4.17	
		TERC	415.9	0.8615	0.8370	0.4308	0.4185	3.7215	3.7090	3.72	
01/06/26	23:42	WASH	38.9	2.4706	4.3468	1.2353	2.1734	2.5454	2.7908	2.67	2.67
		BIRH	83.6	0.3827	0.5768	0.1914	0.2884	2.1809	2.3590	2.27	
		FICH	168.7	0.8697	1.2366	0.4349	0.6183	2.9931	3.1459	3.07	
01/06/27	01:02	WASH	35.3	1.2154	1.2544	0.6077	0.6272	2.1830	2.1968	2.19	2.46
		KARA	127.8	0.4972	0.4154	0.2486	0.2077	2.5623	2.4842	2.52	
		FICH	172	0.3729	0.4046	0.1865	0.2023	2.6389	2.6743	2.66	
01/06/27	01:05	WASH	36.7	9.2815	10.7245	4.6407	5.3622	3.0876	3.1504	3.12	3.4
		FICH	169	1.7945	2.5533	0.8973	1.2767	3.3089	3.4620	3.39	
		DMRK	292.8	1.9607	1.4969	0.9804	0.7485	3.7650	3.6478	3.71	
01/06/27	01:08	WASH	29	0.8376	1.2006	0.4188	0.6003	1.9125	2.0688	1.99	2.16
		FICH	153.5	0.2134	0.2194	0.1067	0.1097	2.3176	2.3296	2.32	
01/06/27	01:14	WASH	31.8	0.3952	0.7713	0.1976	0.3857	1.6371	1.9275	1.78	2.05
		FICH	156.2	0.2111	0.2080	0.1055	0.1040	2.3248	2.3184	2.32	
01/06/27	02:16	WASH	33.7	1.2263	1.9847	0.6132	0.9923	2.1611	2.3702	2.27	2.37
		FICH	173.4	0.2430	0.2509	0.1215	0.1254	2.4585	2.4724	2.47	
01/06/27	02:30	WASH	27.9	0.3441	0.5555	0.1721	0.2777	1.5048	1.7128	1.61	1.87
		FICH	171.4	0.0986	0.1325	0.0493	0.0663	2.0589	2.1871	2.12	
01/06/27	06:00	WASH	29.9	2.2451	5.8415	1.1226	2.9207	2.3575	2.7728	2.57	2.64
		FICH	158.9	0.4683	0.5200	0.2342	0.2600	2.6827	2.7282	2.71	
01/06/27	10:40	WASH	31.7	3.9713	10.1930	1.9857	5.0965	2.6375	3.0469	2.84	2.85
		FICH	158.4	0.6397	0.7593	0.3198	0.3797	2.8159	2.8904	2.85	
01/06/27	15:14	WASH	33.8	12.9684	26.1377	6.4842	13.0689	3.1870	3.4914	3.34	3.41
		FICH	168.9	2.2367	3.2341	1.1184	1.6170	3.4041	3.5643	3.48	
01/06/27	16:30	WASH	35.4	4.4569	10.0177	2.2284	5.0088	2.7489	3.1007	2.92	2.9
		FICH	171.5	0.5852	0.7168	0.2926	0.3584	2.8325	2.9206	2.88	
01/06/27	16:33	WASH	32.7	2.0049	4.4694	1.0025	2.2347	2.3579	2.7060	2.53	2.53
		FICH	172	0.2634	0.3161	0.1317	0.1580	2.4879	2.5671	2.53	
01/06/27	20:38	WASH	32.5	2.1218	2.3098	1.0609	1.1549	2.3791	2.4159	2.40	2.4
		FICH	168.5	0.2434	0.1990	0.1217	0.0995	2.4393	2.3518	2.40	
01/06/28	04:42	WASH	34.6	1.6287	3.2552	0.8143	1.6276	2.2990	2.5997	2.45	2.4
		FICH	153.4	0.2117	0.2443	0.1058	0.1221	2.3137	2.3758	2.34	
01/06/28	07:13	WASH	27.7	3.1284	6.8900	1.5642	3.4450	2.4595	2.8024	2.63	2.69
		FICH	155.8	0.5223	0.6290	0.2611	0.3145	2.7165	2.7972	2.76	
01/06/28	23:48	WASH	38.2	1.0891	2.0025	0.5445	1.0013	2.1795	2.4440	2.31	2.29
		FICH	165.3	0.1555	0.1821	0.0777	0.0911	2.2312	2.2998	2.27	
01/06/29	01:10	WASH	37.8	0.9429	1.2813	0.4715	0.6407	2.1110	2.2442	2.18	2.24
		FICH	160.7	0.1759	0.2136	0.0880	0.1068	2.2652	2.3495	2.31	
01/06/29	10:54	WASH	33.6	1.4080	2.9045	0.7040	1.4522	2.2195	2.5339	2.38	2.48
		FICH	158.8	0.3585	0.3769	0.1792	0.1884	2.5662	2.5879	2.58	
01/06/29	14:44	WASH	36.8	5.6665	10.9111	2.8332	5.4555	2.8749	3.1594	3.02	3.12
		FICH	169.3	1.4447	1.4316	0.7223	0.7158	3.2159	3.2120	3.21	
01/06/30	08:48	WASH	41.3	5.6269	8.6603	2.8134	4.3301	2.9366	3.1238	3.03	3.18

		FICH	171.3	1.7532	1.9857	0.8766	0.9929	3.3082	3.3623	3.34	
01/06/30	09:12	WASH	35.9	1.7806	3.3445	0.8903	1.6723	2.3583	2.6321	2.50	2.65
		FICH	158.6	0.6078	0.6123	0.3039	0.3062	2.7946	2.7978	2.80	
01/07/01	15:16	WASH	38.9	3.8513	9.7867	1.9257	4.8933	2.7382	3.1433	2.94	3.01
		FICH	167.4	1.2066	0.9999	0.6033	0.4999	3.1298	3.0482	3.09	
01/07/01	17:24	WASH	38.5	3.9936	7.4343	1.9968	3.7172	2.7482	3.0181	2.88	2.74
		BIRH	82	0.8137	0.8147	0.4069	0.4073	2.4967	2.4972	2.50	
		FICH	167.1	0.6326	0.6423	0.3163	0.3212	2.8482	2.8548	2.85	
01/07/02	01:37	WASH	40.3	4.7051	13.2473	2.3525	6.6236	2.8451	3.2946	3.07	2.98
		FICH	168.6	0.7071	0.6752	0.3535	0.3376	2.9027	2.8827	2.89	
01/07/02	19:48	WASH	39.6	1.6032	5.0033	0.8016	2.5017	2.3676	2.8619	2.61	2.75
		FICH	170.6	0.7610	0.5707	0.3805	0.2853	2.9429	2.8179	2.88	
01/07/02	21:01	WASH	39.5	2.4913	4.1202	1.2457	2.0601	2.5577	2.7762	2.67	2.58
		FICH	166.9	0.2992	0.2596	0.1496	0.1298	2.5222	2.4605	2.49	
01/07/05	09:49	WASH	38.5	6.6018	11.6423	3.3009	5.8211	2.9665	3.2129	3.09	3.22
		FICH	167.8	2.0228	2.0362	1.0114	1.0181	3.3559	3.3588	3.36	
01/07/05	18:27	BUTA	22.8	4.9630	4.5670	2.4815	2.2835	2.5535	2.5174	2.54	2.55
		FICH	211.1	0.2024	0.2403	0.1012	0.1202	2.5216	2.5962	2.56	
01/07/09	21:03	WASH	30.4	10.3020	17.3542	5.1510	8.6771	3.0283	3.2548	3.14	3.1
		FICH	167.8	1.0174	1.0450	0.5087	0.5225	3.0574	3.0691	3.06	
01/07/09	23:24	WASH	54.5	5.4235	23.2972	2.7118	11.6486	3.0788	3.7119	3.40	3.26
		FICH	150.8	1.6521	1.3582	0.8260	0.6791	3.1943	3.1093	3.15	
		BUTA	239.3	1.3831	1.1277	0.6916	0.5638	3.4515	3.3629	3.41	
		BAHI	374.5	0.2497	0.2422	0.1248	0.1211	3.0850	3.0719	3.08	
01/07/13	22:34	KARA	143.8	3.6106	3.8863	1.8053	1.9431	3.5017	3.5337	3.52	3.36
		DIYA	256.7	0.7225	0.6459	0.3612	0.3230	3.2246	3.1759	3.20	
01/07/17	18:28	BUTA	66.2	3.3632	2.2340	1.6816	1.1170	2.9849	2.8072	2.90	2.76
		BIRH	277.3	0.1760	0.1354	0.0880	0.0677	2.6732	2.5595	2.62	
01/11/06	21:52	TERC	138.6	1.1514	1.1179	0.5757	0.5590	2.9807	2.9679	2.97	3.14
		DELE	309.7	0.5348	0.7208	0.2674	0.3604	3.2480	3.3776	3.31	
01/11/11	22:32	BIRH	30.9	6.0176	8.4182	3.0088	4.2091	2.8038	2.9496	2.88	3.26
		AAUS	110.2	3.4905	2.5257	1.7452	1.2628	3.3128	3.1723	3.24	
		FICH	110.4	1.5341	1.3754	0.7670	0.6877	2.9570	2.9095	2.93	
		DIYA	264.9	0.8352	0.8041	0.4176	0.4021	3.3126	3.2961	3.30	
		TERC	375.2	0.4987	0.3374	0.2494	0.1687	3.3872	3.2175	3.30	
		DELE	385.6	1.2032	1.7294	0.6016	0.8647	3.7950	3.9525	3.87	
01/11/11	22:38	BIRH	30.5	49.6569	117.8083	24.8284	58.9042	3.7132	4.0884	3.90	3.9
		AAUS	109.4	7.0240	7.7559	3.5120	3.8780	3.6119	3.6550	3.63	
		FICH	109.7	6.7943	6.3222	3.3972	3.1611	3.5992	3.5679	3.58	
		DIYA	265	9.1464	8.2629	4.5732	4.1315	4.3524	4.3082	4.33	
		TERC	374.5	1.3964	0.7912	0.6982	0.3956	3.8326	3.5859	3.71	
		DELE	384.7	2.9359	4.2556	1.4680	2.1278	4.1802	4.3414	4.26	
01/11/14	06:09	TERC	120	3.2157	3.3492	1.6079	1.6746	3.3320	3.3496	3.34	3.79
		JIMA	156.2	7.9375	10.4741	3.9687	5.2371	3.9000	4.0205	3.96	
		DELE	267.9	5.3294	4.0728	2.6647	2.0364	4.1265	4.0098	4.07	
01/11/17	21:29	TERC	93.6	1.0436	0.6164	0.5218	0.3082	2.6859	2.4572	2.57	2.39
		HERO	139.2	0.1930	0.2024	0.0965	0.1012	2.2079	2.2285	2.22	
01/11/23	14:45	WASH	40	16.3099	16.6375	8.1549	8.3188	3.3808	3.3894	3.39	3.54
		FURI	149.9	4.3919	6.3474	2.1960	3.1737	3.6149	3.7748	3.69	

		BAHI	378.8	0.5029	0.9482	0.2514	0.4741	3.3996	3.6751	3.54	
		FICH	146.5	3.5616	4.4391	1.7808	2.2196	3.5083	3.6040	3.56	
01/11/24	13:03	FICH	37.5	3.0346	4.4743	1.5173	2.2371	2.6142	2.7828	2.70	2.83
		BAHI	261.8	0.3497	0.4006	0.1748	0.2003	2.9251	2.9841	2.95	
01/11/25	09:20	WASH	39.4	4.2227	2.9321	2.1114	1.4661	2.7854	2.6270	2.71	2.88
		KARA	123.2	1.2307	1.1079	0.6154	0.5540	2.9320	2.8863	2.91	
		FICH	149.1	1.0583	1.2478	0.5292	0.6239	2.9932	3.0647	3.03	
01/11/26	20:59	HOSA	14.3	9.6407	8.6994	4.8204	4.3497	2.5903	2.5457	2.57	2.49
		GUDE	142.8	0.2930	0.3099	0.1465	0.1549	2.4062	2.4306	2.42	
01/12/12	13:33	BIRH	28.3	0.6472	0.7563	0.3236	0.3782	1.7870	1.8547	1.82	2.15
		FURI	125.9	1.0510	0.5687	0.5255	0.2844	2.8775	2.6108	2.74	
		FICH	108.7	0.1669	0.1041	0.0835	0.0520	1.9838	1.7787	1.88	
01/12/13	02:14	BIRH	29.8	4.0733	5.9891	2.0366	2.9946	2.6143	2.7818	2.70	3.1
		FURI	126.1	9.2292	5.7162	4.6146	2.8581	3.8221	3.6141	3.72	
		FICH	110	1.3840	0.7969	0.6920	0.3985	2.9099	2.6702	2.79	
		BAHI	343.4	0.4504	0.3375	0.2252	0.1687	3.2630	3.1376	3.20	
01/12/23	22:33	SELA	52.2	0.2245	0.4988	0.1123	0.2494	1.6710	2.0176	1.84	1.99
		HOSA	96.6	0.3080	0.2665	0.1540	0.1332	2.1755	2.1126	2.14	

APPENDIX B– Catalogue of earthquakes located in this study

DATE – Date of the event (year/month/day)

OR. TIME – Event origin time in GMT (Hour:Minute:Second)

LAT. – Latitude of the earthquake epicenter in degrees

LON. – Longitude of the earthquake epicenter in degrees

ML – Local magnitude

DATE	OR. TIME	LAT. (^{O})	LON. (^{O})	DEPTH (KM)	ML
01/05/10	16:51:08.02	9.1925	38.4107	0.03	2.8
01/05/11	17:29:48.81	5.2577	37.5945	6.69	3.3
01/05/12	01:44:14.01	9.5558	39.5860	8.39	3.2
01/05/12	02:06:41.89	9.5467	39.5830	6.84	3.3
01/05/14	23:10:59.73	9.4902	39.5343	1.28	2.9
01/05/18	13:49:01.08	9.4765	39.7010	11.68	2.6
01/05/18	18:07:51.68	5.7922	36.5412	25.13	4.2
01/05/18	20:32:57.43	7.6875	38.0048	11.24	2.3
01/05/19	03:28:17.56	9.1818	40.0475	22.91	2.6
01/05/19	11:18:22.71	9.1948	40.0328	19.01	2.9
01/05/19	18:49:23.11	12.1588	42.3108	7.00	3.9
01/05/20	09:58:00.78	9.1855	40.0143	14.10	2.8
01/05/21	19:23:51.28	9.2468	40.0118	11.92	2.4
01/05/21	20:09:13.49	9.4777	39.7030	22.95	2.2
01/05/21	21:12:43.15	7.6988	37.9807	11.54	2.2
01/05/22	03:49:49.58	9.3817	40.2378	2.99	2.4
01/05/22	16:10:21.54	9.2148	40.0108	13.59	2.7
01/01/23	01:16:08.45	9.4815	39.4225	12.74	3.4
01/01/24	08:09:49.99	9.5145	39.7127	15.48	2.7
01/05/24	19:55:16.29	9.2285	40.0247	15.00	2.2
01/05/24	20:24:35.29	9.4848	39.4215	10.79	1.7

01/05/24	21:14:20.68	9.1843	39.6599	14.32	2.1
01/05/24	21:19:24.08	9.1833	39.1000	15.95	2.3
01/05/24	21:25:53.46	9.1325	40.1028	31.29	2.6
01/05/25	18:28:00.40	9.2147	40.0067	13.13	2.4
01/05/25	21:05:41.83	9.1212	39.9458	14.91	2.3
01/05/25	22:19:25.22	13.2798	39.0693	7.00	3.6
01/05/26	20:10:45.13	11.7263	41.4940	27.57	3.3
01/05/28	06:42:05.11	9.2170	40.0325	17.60	3.4
01/05/30	20:19:12.48	9.2342	40.0282	14.59	3.1
01/05/30	22:38:07.76	9.2363	40.0222	11.03	2.2
01/06/02	23:09:57.05	6.5493	37.7117	13.68	2.7
01/06/04	11:38:25.37	9.3198	40.1805	9.78	2.5
01/06/04	22:56:17.21	9.3397	40.2082	8.27	3.1
01/06/04	23:12:19.64	9.3478	40.1949	8.56	3.0
01/06/05	01:58:38.82	9.3508	40.1813	3.00	2.7
01/06/08	01:25:05.78	11.8310	40.9040	2.92	3.0
01/06/08	07:47:34.90	12.6262	40.7695	7.00	2.9
01/06/09	04:59:58.82	11.8925	39.6677	5.13	3.1
01/06/10	02:53:37.53	11.8767	39.6910	7.00	2.9
01/06/14	00:47:55.02	6.8470	38.2047	11.16	2.9
01/06/14	05:16:12.96	9.7003	39.7383	11.09	2.6
01/06/14	23:32:23.94	7.9238	38.7333	7.00	2.1
01/06/15	00:19:20.38	8.4555	38.4167	22.10	2.6
01/06/17	23:23:14.24	9.3300	40.2065	11.10	2.2
01/06/17	23:24:31.10	9.3288	40.2097	10.78	2.5
01/06/17	23:54:52.46	9.3270	40.2115	10.91	2.6
01/06/18	00:18:42.65	9.3325	40.2057	12.32	2.6
01/06/19	22:56:25.52	9.3170	40.1803	5.44	2.8
01/06/20	12:33:42.87	9.8003	39.6573	6.70	1.8
01/06/22	11:27:04.62	9.3023	40.2012	11.81	2.6
01/06/22	14:09:23.04	9.1940	40.0027	11.39	2.7

01/06/22	14:18:46.86	9.2501	40.0775	9.67	2.5
01/06/22	14:52:28.00	9.3457	40.1872	10.85	2.9
01/06/22	23:39:56.52	9.3240	40.2182	10.33	3.6
01/06/23	05:42:30.03	9.2453	40.0545	10.34	2.3
01/06/23	13:20:38.29	9.3167	40.2152	10.98	3.4
01/06/23	19:09:05.88	9.3414	40.2248	4.68	3.7
01/06/23	19:12:06.48	9.3355	40.2192	6.29	3.8
01/06/23	19:16:05.33	9.3078	40.2240	12.59	2.9
01/06/23	19:29:14.50	9.1707	40.2007	7.00	2.4
01/06/23	20:00:21.40	9.3311	40.2275	13.17	4.1
01/06/24	01:47:19.32	9.3414	40.2019	7.61	3.1
01/06/24	02:19:38.74	9.3160	40.1498	3.51	3.1
01/06/24	03:53:22.57	9.3233	40.2065	5.04	3.1
01/06/24	05:24:42.14	9.2037	40.5572	7.00	2.8
01/06/24	07:26:36.13	9.3490	40.2420	10.98	2.9
01/06/24	10:42:27.94	9.2938	40.1830	12.66	2.1
01/06/24	10:46:02.67	9.3338	40.2555	11.98	3.2
01/06/24	10:54:51.93	9.2942	40.1112	4.08	2.4
01/06/24	13:21:38.17	9.2325	40.0403	11.15	2.9
01/06/24	18:17:27.56	9.3157	40.2213	12.03	2.8
01/06/24	18:22:56.66	9 .3372	40.2240	4.48	2.9
01/06/24	19:26:43.65	9.2862	40.1373	10.95	2.1
01/06/24	20:25:40.19	9.3223	40.2472	15.49	2.2
01/06/25	00:41:43.59	9.2653	40.2143	25.71	2.3
01/06/25	00:47:27.79	9.3404	40.2250	9.79	2.9
01/06/25	06:58:07.33	9.3513	40.2233	24.64	3.2
01/06/25	07:09:32.95	9.3360	40.2300	10.81	2.6
01/06/25	07:16:42.38	9.3098	40.1597	11.11	2.7
01/06/25	07:37:51.53	9.3388	40.2162	11.18	2.9
01/06/25	08:14:16.21	9.3337	40.1670	3.03	2.6
01/06/25	08:26:16.82	9.3370	40.2188	11.07	3.2

01/06/25	09:14:45.15	9.3352	40.2300	13.02	3.5
01/06/25	09:46:06.47	9.2927	40.1297	7.98	3.1
01/06/25	10:20:49.15	9.2842	40.0963	5.66	2.5
01/06/25	11:08:46.00	9.2922	40.1250	10.00	2.7
01/06/25	16:38:02.60	9.3382	40.2522	11.25	2.9
01/06/25	16:39:47.84	9.3337	40.2192	11.73	2.9
01/06/25	16:52:58.16	9.3410	40.1908	10.79	2.4
01/06/25	16:56:34.80	9.3428	40.2175	14.11	2.3
01/06/25	16:59:51.84	9.3435	40.2395	11.26	2.8
01/06/25	17:02:59.44	9.3323	40.2280	11.00	3.4
01/06/25	17:36:09.95	9.3395	40.2618	14.47	2.7
01/06/26	12:46:51.83	9.3212	40.1690	12.31	2.9
01/06/26	17:33:21.53	9.3395	40.1793	7.36	3.1
01/06/26	17:39:50.58	9.3462	40.2171	9.19	3.3
01/06/26	22:15:42.39	9.3300	40.1770	15.31	2.3
01/06/26	22:22:04.04	9.3536	40.2236	11.74	3.7
01/06/26	22:32:16.89	9.3468	40.2249	11.01	3.9
01/06/26	23:42:20.30	9.3510	40.2036	16.56	2.7
01/06/27	01:01:53.20	9.3033	40.2272	17.56	2.5
01/06/27	01:04:58.81	9.3240	40.2113	8.61	3.4
01/06/27	01:08:34.93	9.1983	40.0055	11.01	2.2
01/06/27	01:14:18.92	9.2567	40.0580	10.97	2.1
01/06/27	02:16:10.16	9.2865	40.2355	19.93	2.4
01/06/27	02:30:20.28	9.2403	40.1993	24.95	1.9
01/06/27	06:00:09.53	9.2470	40.0802	9.17	2.6
01/06/27	10:40:15.09	9.2642	40.0820	3.70	2.8
01/06/27	15:14:18.14	9.2938	40.1947	10.80	3.4
01/06/27	16:30:32.13	9.3052	40.2228	12.04	2.9
01/06/27	16:33:03.18	9.2810	40.2203	13.94	2.5
01/06/27	20:38:48.63	9.2832	40.1870	11.37	2.4
01/06/28	04:42:47.08	9.2755	40.0373	8.18	2.4

01/06/28	07:13:49.70	9.2005	40.0292	10.81	2.7
01/06/28	23:48:27.84	9.3352	40.1735	11.03	2.3
01/06/29	01:10:48.80	9.3302	40.1282	3.64	2.2
01/06/29	10:54:15.87	9.2848	40.0933	3.99	2.5
01/06/29	14:44:25.27	9.3200	40.2070	13.42	3.1
01/06/30	08:47:58.28	9.3642	40.2384	11.47	3.2
01/06/30	09:12:22.20	9.3080	40.1002	3.51	2.6
01/07/01	15:15:55.14	9.3402	40.1953	5.41	3.0
01/07/01	17:24:49.10	9.3373	40.1917	11.15	2.7
01/07/02	01:37:32.07	9.3498	40.2218	12.17	2.9
01/07/02	19:48:33.78	9.3427	40.2265	12.25	2.7
01/07/02	21:00:56.03	9.3460	40.1925	12.08	2.6
01/07/05	09:49:05.66	9.3368	40.1978	7.65	3.2
01/07/05	18:27:42.23	7.9148	38.3397	7.00	2.5
01/07/09	21:03:17.14	9.2592	40.1926	10.58	3.1
01/07/09	23:24:05.90	9.4742	40.0757	11.45	3.3
01/07/13	22:34:13.39	9.6153	38.9062	0.01	3.4
01/07/17	18:28:28.99	7.7465	37.9108	3.26	2.7
01/11/06	21:52:35.79	6.1077	37.8787	41.04	3.1
01/11/11	22:32:40.60	9.4414	39.6822	9.44	3.3
01/11/11	22:38:01.08	9.4403	39.6751	9.99	3.9
01/11/14	06:09:20.87	6.9537	38.2440	0.05	3.8
01/11/17	21:28:53.33	7.0545	38.0172	6.41	2.4
01/11/23	14:45:32.86	9.3018	39.9807	13.02	3.5
01/11/24	13:03:38.59	9.5003	38.5468	11.17	2.8
01/11/25	09:20:28.36	9.3103	40.0088	11.87	2.9
01/11/26	20:59:49.02	7.6753	37.7905	0.58	2.5
01/12/12	13:33:53.47	9.4630	39.6737	11.75	2.1
01/12/13	02:14:39.00	9.4493	39.6815	11.00	3.1
01/12/23	22:33:35.58	7.7565	38.7112	11.07	2.0

REFERENCES

Acocela, V and Korme, T. (2002) Holocene extension direction along the Main Ethiopian Rift, East Africa. *Terra Nova*, 14, 191 - 197.

Aki, k. (1965) Maximum Likelihood Estimate of b in the Formula log N = a – bM and its confidence Limits. *Bull. Earthq. Res. Inst.*, 43, pp. 237 - 239.

Aki, K. and Richards, P.G. (1980) Quantitative Seismology: Theory and Methods. Volume I.

Anderson, J.A. and Wood, H.O. (1925) Description and theory of the torsion seismometer. *Bull. Seism. Soc. Am.,* 15, 1-72.

Ayele, A. (1995) Earthquake catalogue of the Horn of Africa for the period 1960 – 1993. *Seismological Dept.,U*ppsala Univ., Report, 3-95, 1-9.

Ayele, A. (2000) Normal left-oblique fault mechanisms as an indication of sinistral deformation between Nubia and Somalia plates in the Main Ethiopian Rift. *J. Afr. Earth Sc.*, 31 (2), 359-367.

Ayele, A. and Arvidsson, R. (1998) Fault mechanisms and tectonic implication of the 1985-1987 earthquake sequence in south-western Ethiopia. *J. Seismology,*1, 383-394.

Ayele, A. and Kulhanek, O. (2000) Reassessment of source parameters for three major earthquakes in the East African rift system from historical seismograms and bulletins. *Annali Di Geofisica,* 43, 81 – 94.

Ayele, A. and Kulhanek, O. (1997) Spatial and temporal variation of seismicity in the Horn of Africa from 1960 to 1993. *Geophys. J. Int.*, 130, 805-810.

Ayele, A., Nyblade, A.A, Langston, C.A., Cara, M. and Leveque, J. (2006) New evidence for Afro-Arabian plate separation in southern Afar. *In*: Yirgu, G., Ebinger, C.J., and Maguire, P.K.H. (eds) *The Afar volcanic province within the east African Rift system. Geol. Soc.* London, Special Publications, 259, 133-141.

Ayele, A., Stuart, G., Bastow, I. and Keir, D. (2007) The August 2002 earthquake sequence in north Afar: Insights into the neotectonics of the Danakil microplate. *J. Afr. Earth Sc.,* 48, 70 – 79.

Bastow, I., Stuart, G., Kendall, M. and Ebinger, C.J. (2005) Upper mantle seismic structure in a region of incipient continental break-up: northern Main Ethiopian Rift. *Geoph. J. Int.*, 162, 479 – 493.

Bilham, R., Bendick, R., Larson, K., Mohr, P., Braun, J., Tesfaye, S. and Asfaw, L.M. (1999) Secular and tidal strain across the Ethiopian Rift. *Geoph. Res. Lett.*, 26, 2789 - 2792.

Boccaletti, M., Bonini, M., mazzuoli, R., Abebe, B., Piccardi, L. and Tortorici, L. (1998) Quaternary oblique extensional tectonics in the Ethiopian Rift (Horn of Africa). *Tectonophysica*, 287, 97 – 116.

Boccaletti, M., Mazzuoli, R., Bonini, M., Trua, T. and Abebe, B. (1999) Plio-Quaternary volcanotectonic activity in the northern sector of the Main Ethiopian Rift: Relationships with oblique rifting. *J. Afr. Earth Sc.*, 29, 679 – 698.

Casey, M., Ebinger, C.J., Keir, D., Gloaguen, R. and mohamed, F. (2006) Strain accommodation in transitional rifts: extension by magma intrusion and faulting in Ethiopian rift magmatic segments. *In*: Yirgu, G., Ebinger, C.J., and Maguire, P.K.H. (eds) *The Afar volcanic province within the east African Rift system. Geol. Soc.* London, Special Publications, 259, 143 - 163.

Chorowicz, J., Collet, B., Bonavia, F.F. and Korme, T. (1994). Northwest to north-northwest extension direction in the Ethiopian Rift deduced from the orientation of extension structures and fault-slip analysis. *Bull. Geol. Soc. Am.*, 105, 1560–1570.

Chu, D. and Gordon, R. (1999) Evidence for motion between Nubia and Somalia along the Southwest Indian ridge. *Nature*, 398, 64 – 66.

Daly, E., Keir, D., Ebinger, C.J., Stuart, G., Ayele, A. and Waltham, D. (2004) Crustal structure of the northern Main Ethiopian rift from a tomographic inversion of local earthquakes. *In*: Yirgu, *et al*. (eds) *Proceedings of International Conference on the East African Rift System*, June 20-24 2004, Addis Ababa, Ethiopia: Ethiopian Geoscience and Mineral Engineering Association, p 51-52.

Dugda, M., Nyblade, A.A., Julia, J., Langston, C.A., Ammon, C.J. and Simiyu, S. (2005) Crustal structure in Ethiopia and Kenya from receiver function analysis: Implications for rift development in eastern Africa. *J. Geoph. Res.,* 110, doi 10.1029/2004JB003065.

Ebinger, C.J. and Casey, M. (2001) Continental breakup in magmatic provinces: an Ethiopian example. *Geol.*, 29, 527 - 530.

Ebinger, C.J. and Sleep, N.H. (1998) Cenozoic magmatism throughout east Africa resulting from the impact of a single plume. *Nature*, 395, 788 – 791.

Ebinger, C.J., Yemane, T., Harding, D., Tesfaye, S., Rex, D. and Kelly, S. (2000) Rift deflection, migration, and propagation: Linkage of the Ethiopian and eastern rifts, Africa. *Geol. Soc. Am. Bull.*, 102, 163 – 176.

Garfunkel, Z. and Beyth, M. (2006) Constraints on the structural development of Afar imposed by the kinematics of the major surrounding plates. *In*: Yirgu, G., Ebinger, C.J., and Maguire, P.K.H. (eds) *The Afar volcanic province within the east African Rift system. Geol. Soc.* London, Special Publications, 259, 23 - 42.

Gouin, P. (1979) Earthquake history of Ethiopia and the Horn of Africa. International Development Research Center, Ottawa, Ont., pp. 258.

Gutenberg, B. and Richter, C.F. (1956) Earthquake magnitude, intensity, energy, and acceleration. *Bull. Seism. Soc. Am.,* 46, 105-145.

Havskov, J. and Ottemoller, L. (2000). SEISAN: The Earthquake Analysis Software. *Inst. Solid Earth Physics*, Univ. Bergen.

Hayward, N. and Ebinger, C.J. (1996) Variations in along-axis segmentation of the Afar rift system, *tectonics*, 15, 244 – 257.

Hofmann, C., Courtillot, V., Feraud, G., Rochette, P., Yirgu, G., Ketefo, E. and Pik, R. (1997) Timing of the Ethiopian flood basalt event and implications for plume birth and global change. *Nature*, 389, 838 – 841.

Hofstetter, R. and Beyth, M. (2003). The Afar Depression: interpretation of the 1960 – 2000 earthquakes. *Geoph. J. Int.*, 155, 715 – 732.

Kebede, F. (1989) Seismotectonics of the East African rift system north of 12^{o}S to southern Red Sea. *Seismological Dept.*, Uppsala Univ., Report No. 1-89, pp. 34.

Kebede, F., Kim, W.-Y. and Kulhaek, O. (1989) Dynamic source parameters of the March-May 1969 Serdo earthquake sequence in Central Afar, Ethiopia, deduced from teleseismic body waves. *J. Geoph. Res.*, 94, 5603 – 5614.

Kebede, F. and Kulhanek, O. (1991) Recent seismicity of the East African rift system and its implications. *Phys. Earth Planet Inter.*, 68, 259-273.

Kebede, F. and Kulhanek, O. (1994) Spatial and temporal variations in b-values along the East African rift system and the southern Red Sea. *Phys. Earth Planet Inter.*, 83, 249-264.

Keir, D. (2006) Catalogue of earthquake epicenters located with 1-D velocity model. *In*: Strain accommodation by magmatism and faulting as rifting proceeds to breakup: Seismicity of the Northern Ethiopian Rift. PhD Dissertation, pp. 110 – 133.

Keir, D., Ebinger, C.J., Stuart, G., Daly, E. and Ayele, A. (2006a) Strain accommodation by magmatism and faulting as rifting proceeds to breakup: Seismicity of the northern Ethiopian Rift. *J. Geoph.Res.,* 111, B05314, doi:1029/2005JB 003748.

Keir, D., Stuart, G.W., Jackson, A. and Ayele, A (2006b) Local earthquake magnitude scale and seismicity rate for the Ethiopian rift. *Bull. Seism. Soc. Am.,* 96, 1-10.

Keranen, K., Klemperer, S., Gloaguen, R. and EAGLE working group. (2004) Three-dimensional imaging of a protoridge axis in the Main Ethiopian Rift. *Geol.,* 39, 949 – 952.

Klein, F.W. (2002) User;s guide to Hypoinverse-2000, a Fortran program to solve for earthquake locations and magnitudes. *USGS Open File Report*, 02-171, 1-123.

Korme, T., Chorowicz, J., Collet, B. and Bonavia, F.F., 1997. Volcanic vents rooted on extension fractures and their geodynamic implications in the Ethiopian Rift. *J. Volcanol. Geotherm. Res.*, 79, 205–222.

Lay, T. and Wallace, T.C. (1995) Modern global seismology. Academic Press San Diego, California.

Lowrie, W. (1997) Fundamentals of Geophysics. Cambridge University Press.

Mackenzie, G., Thybo, H. and Maguire, P.K.H. (2005) Crustal velocity structure across the Main Ethiopian Rift: Results from two-dimensional wide-angle seismic modelling. *Geoph. J. Int*, 162, 994 - 1006.

Maguire, P.K.H., Keller, G.R. *Et al*. (2006) Crustal structure of the northern Main Ethiopian Rift from the EAGLE controlled-source survey; a snap shot of incipient lithospheric break-up. *In*: Yirgu, G., Ebinger, C.J., and Maguire, P.K.H. (eds) *The Afar volcanic province within the east African Rift system. Geol. Soc.* London, Special Publications, 259, 269 - 291.

Mahatsente, R., Jenztsch, G. and Jahr, T. (1999) Crustal structure of the Main Ethiopian Rift from gravity data: 3-dimensional modelling. *Tectonophysics*, 313, 363 - 382.

McKenzie, D.P., Davies, D. and Molnar, P., 1970. Plate tectonics of the Red Sea and East Africa. *Nature*, 226, 243–248.

Manighetti, I., Tapponnier, P., Courtillot, V., Gruszow, S. and Gillot, P.-Y (1997) Propagation of rifting along the Arabia-Somalia plate boundary: The gulfs of Aden and Tadjoura. *J. Geophys. Res.*, 102, 2681 - 2710.

Menke, W. (1987) Geophysical data analysis: Discrete inverse theory. Academic press, New York.

Meyer, W., Pilger, A., Rosler, A. and Stets, J. (1975) Tectonic evolution of the northern part of the Main Ethiopian. *In*: Pilger, A and Rosler, A. (eds) *Afar Depression of Ethiopia*, Schweizerbart, Stuttgart.

Mohr, P.A. (1967) The Ethiopian Rift system. *Bull. Geoph. Obser. Addis Ababa* 11, 1 – 65.

Mohr, P.A. (1987) Patterns of faulting in the Ethiopian Rift Valley. *Tectonophysics*, 143, 169 – 179.

Nyblade, A.A. and Langston, C.A. (2002) Broadband Seismic experiments probe in East African rift. *Eos Trans. AGU,* 83, 405-410.

Schilling, J.-G, Kingsley, R., Hanan, B. and McCully, B. (1992) Nd-Sr-Pb isotopic variations along the Gulf of Aden: Evidence for the Afar mantle plume-lithosphere interaction. *J. Geophys. Res.*, 97, 10927 – 10966.

Shi, Y. and Bolt, B.A. (1982) The standard error of the magnitude-frequency b-value. *Bull. Seism. Soc. Am.*, 72, 1677 – 1687.

Snoke, J.A., Munsey, A.C., Teague, A.C. and Bollinger, G.A. (1984) A program for focal mechanism determination by combined use of polarity and SV-P amplitude ratio data. *Earthquake notes*, 15(3).

Stuart, G., Bastow, I. and Ebinger., C.J. (2006) Crustal structure of the northern Main Ethiopian Rift from receiver function studies. *In*: Yirgu, G., Ebinger, C.J. and Maguire, P.K.H. (esd) *The Afar volcanic province within the East African Rift system. Geol. Soc.,* London, special publications, 259, 253 – 267.

Tiberi, C., Ebinger, C.J., Ballu, V., Stuart, G. and Oluma, B. (2005) Inverse models of gravity data from the Red Sea-Aden-East African rifts triple junction zone. *Geoph. J. Int.*, 163, 775 - 787.

Ukstins, I., Rene, P., Wolfenden, E., Baker, J., Ayalew, D. and Menzies, M. (2002) Matching conjugate volcanic rifted margins: $^{40}Ar/^{39}Ar$ chronostratigraphy of pre- and syn-rift bimodal flood volcanism in Ethiopia and Yemen. *Earth and Planet. Sc. Lett.*, 198, 289 – 306.

Waldhauser, F. and Ellsworth, W.L. (2000) A Double-Difference earthquake location algorithm: method and application to the Northern Hayward Fault, California. *Bull. Seismological Soc. Am,* 90, 6, 1353-1368.

WoldeGabriel, G., Aronson, J. and Walter, R. (1990) Geology, geochronology, and rift basin development in the central sector of the Main Ethiopian Rift. *Geol. Soc. Am. Bull.*, 102, 439 - 458.

Wolfenden, E., Ebinger, C.J., Yirgu, G., Deino, A. and Ayalew, D. (2004) Evolution of the northern Main Ethiopian Rift: Birth of a triple junction. *Earth and Planet. Sc. Lett.*, 224, 213 – 228.

Wolfenden, E., Ebinger, C.J., Yirgu, G., Renne, P. and Kelley, S.P. (2005) Evolution of the southern Red Sea rift: Birth of a magmatic margin. *Bull. Geol. Soc. Am.*, 117, 846 – 864.

DECLARATION AND COPYRIGHT

I, **Manahloh Belachew**, declare that this thesis is my original work and has not been presented for a degree in any other university, and that all sources of material used for the thesis have been duly acknowledged.

_____	_____
Manahloh Belachew	Dr. Atalay Ayele
	(Advisor)